NeuroImage: Clinical 7 (2015) 424–437

Contents lists available at ScienceDirect

NeuroImage: Clinical

journal homepage: www.elsevier.com/locate/ynicl

Improved nTMS- and DTI-derived CST tractography through anatomical ROI seeding on anterior pontine level compared to internal capsule

Carolin Weiss[a,1,*], Irada Tursunova[a,1], Volker Neuschmelting[a], Hannah Lockau[d], Charlotte Nettekoven[b], Ana-Maria Oros-Peusquens[b], Gabriele Stoffels[b], Anne K. Rehme[b,c], Andrea Maria Faymonville[a], N. Jon Shah[b,e], Karl Josef Langen[b], Roland Goldbrunner[a], Christian Grefkes[b,c]

[a] Department of Neurosurgery, University of Cologne, Cologne 50924, Germany
[b] Institute of Neuroscience and Medicine, Research Centre Jülich, Jülich 52425, Germany
[c] Department of Neurology, University of Cologne, Cologne 50924, Germany
[d] Department of Radiology, University of Cologne, Cologne 50937, Germany
[e] Department of Neurology, University Clinic Aachen, RWTH Aachen University, Aachen 52074, Germany

ARTICLE INFO

Article history:
Received 11 September 2014
Received in revised form 7 January 2015
Accepted 8 January 2015
Available online 20 January 2015

Keywords:
nTMS
DTI
CST
Fractional anisotropy
Somatotopic
ROI

ABSTRACT

Imaging of the course of the corticospinal tract (CST) by diffusion tensor imaging (DTI) is useful for function-preserving tumour surgery. The integration of functional localizer data into tracking algorithms offers to establish a direct structure–function relationship in DTI data. However, alterations of MRI signals in and adjacent to brain tumours often lead to spurious tracking results. We here compared the impact of subcortical seed regions placed at different positions and the influences of the somatotopic location of the cortical seed and clinical co-factors on fibre tracking plausibility in brain tumour patients.

The CST of 32 patients with intracranial tumours was investigated by means of deterministic DTI and neuronavigated transcranial magnetic stimulation (nTMS). The cortical seeds were defined by the nTMS hot spots of the primary motor area (M1) of the hand, the foot and the tongue representation. The CST originating from the contralesional M1 hand area was mapped as intra-individual reference. As subcortical region of interests (ROI), we used the posterior limb of the internal capsule (PLIC) and/or the anterior inferior pontine region (aiP). The plausibility of the fibre trajectories was assessed by a-priori defined anatomical criteria. The following potential co-factors were analysed: Karnofsky Performance Scale (KPS), resting motor threshold (RMT), T1-CE tumour volume, T2 oedema volume, presence of oedema within the PLIC, the fractional anisotropy threshold (FAT) to elicit a minimum amount of fibres and the minimal fibre length.

The results showed a higher proportion of plausible fibre tracts for the aiP-ROI compared to the PLIC-ROI. Low FAT values and the presence of peritumoural oedema within the PLIC led to less plausible fibre tracking results. Most plausible results were obtained when the FAT ranged above a cut-off of 0.105. In addition, there was a strong effect of somatotopic location of the seed ROI; best plausibility was obtained for the contralateral hand CST (100%), followed by the ipsilesional hand CST (>95%), the ipsilesional foot (>85%) and tongue (>75%) CST. In summary, we found that the aiP-ROI yielded better tracking results compared to the IC-ROI when using deterministic CST tractography in brain tumour patients, especially when the M1 hand area was tracked. In case of FAT values lower than 0.10, the result of the respective CST tractography should be interpreted with caution with respect to spurious tracking results. Moreover, the presence of oedema within the internal capsule should be considered a negative predictor for plausible CST tracking.

Abbreviations: aiP, anterior inferior pons; ANOVA, analysis of variance; AUC, area under the curve; APB, abductor pollicis brevis muscle; BOLD, blood oxygenation level dependent; CST, corticospinal tract; DTI, diffusion tensor imaging; FACT, fibre assignment by continuous tracking; FA(T), fractional anisotropy (threshold); FWE, family-wise error; FOV, field-of-view; FMRI, functional magnetic resonance imaging; KPS, Karnofsky performance scale; LDA/C, linear discriminant analysis/coefficient; LT, lateral tongue muscle, anterior third; M1, primary motor cortex; MEP, motor evoked potential; MFL, minimal fibre length; MPRAGE, magnetization prepared rapid acquisition gradient echo (T1 MR sequence); nTMS, neuronavigated transcranial magnetic stimulation; OR, odd's ratio; PLIC, posterior limb of the internal capsule; PM, plantar muscle; RMT, resting motor threshold; ROI, region-of-interest; SD, standard deviation; SE, standard error; X-sq, X-squared (Pearson's chi-square test); p_{xsq}, p-value according to Pearson's chi-square test.

* Corresponding author at: Klinik für Allgemeine Neurochirurgie. Uniklinik Köln, Bettenhaus Eb. 8. Kerpener Str. 62, 50931 Cologne, Germany. Tel.: +49 (0)221 478 97711/0; fax: +49 (0)221 478 6257.
E-mail address: carolin.weiss@uk-koeln.de (C. Weiss).
[1] Both authors contributed equally (shared first-authorship).

http://dx.doi.org/10.1016/j.nicl.2015.01.006

1. Introduction

The introduction of diffusion tensor imaging (DTI) as a non-invasive technique to reconstruct white matter tracts from diffusion-weighted magnetic resonance images (DWI) has opened new vistas onto the structural connectivity in the living human brain in both healthy subjects and patients with brain lesions (Strick and Preston, 1983; Petrides and Pandya, 1984; Barbas and Pandya, 1987; Matelli et al., 1989; Orioli and Strick, 1989; Le Bihan et al., 2001; Barone et al., 2014). Of great clinical importance is to use DTI-based tractography for the planning of neurosurgical interventions in patients with eloquently located brain tumours, e.g. lesions in the vicinity of the primary motor cortex, in order to minimize operation-induced functional deficits (Mori et al., 1999, 2002; Nagae-Poetscher et al., 2004). A common procedure is to place a region-of-interest (ROI) in the primary motor cortex (M1) as starting point for tractography. However, tractography in brain tumour patients can be severely distorted by the disruption of fibre organization, e.g., as a result of tumour infiltration or perilesional oedema (Schonberg et al., 2006; Zolal et al., 2013; Mandelli et al., 2014). Such effects may lead to a decrease of the directionality of the diffusion process and, thus, of the fractional anisotropy (FA) and to spurious tracking results and possibly less accurate operation outcomes (Basser and Pierpaoli, 1996, 1998; Pajevic and Pierpaoli, 1999). One way to overcome invalid tracking results for the motor system is to use a second region-of-interest (ROI) along the corticospinal tract.

Obviously, a critical factor for obtaining valid tracking results is the location of the seed regions. Several groups attempted to optimize the definition of a cortical seed ROI through the integration of functional imaging data into the tracking algorithm. The approach of combining functional imaging and DTI was first introduced using functional magnetic resonance imaging (fMRI) (Guye et al., 2003; Hendler et al., 2003; Watts et al., 2003; Parmar et al., 2004; Schonberg et al., 2006; Staempfli et al., 2008; Zhu et al., 2012). However, fMRI as localizer technique is problematic in conditions where the haemodynamic response and/or neurovascular coupling are altered, e.g., in tumour-infiltrated regions, which may lead to both false positive and false negative BOLD activities (Lehéricy et al., 2000; Wengenroth et al., 2011; Wehner, 2013). Furthermore, fMRI localizer tasks require the active participation of the subject, which is often limited in patients suffering from neurological deficits like hemiparesis. Hence, neuronavigated transcranial magnetic stimulation (nTMS) has been introduced as an alternative to fMRI with respect to the definition of a cortical seed ROI (Frey et al., 2012; Krieg et al., 2012). Here, based on structural MRI scans and continuous detection of the position of the subject's head, motor-evoked potentials (MEPs) at peripheral muscles are systematically induced upon precise nTMS of M1 (Basser, 1994; Ilmoniemi et al., 1999; Basser and Roth, 2000; Picht et al., 2009; Picht et al., 2011, 2012). Hence, nTMS mappings are less dependent on the compliance of the subject compared to fMRI localizer tasks with respect to task performance and/or head movement artefacts, which is especially advantageous in patient populations (Frey et al., 2012; Krieg et al., 2012).

There is, however, little consensus where — along the course of the CST — to place a second ROI. Two alternative positions have been suggested, one at the level of the internal capsule (posterior limb; Han et al., 2010; Holodny et al., 2005a and 2005b; Pan et al., 2012) and the other at the level of the brain stem (usually midbrain) (Gerardin et al., 2003; Lazar et al., 2003; Nimsky et al., 2006; Frey et al., 2012). However, thus far, it remains unknown which of the two positions yield more accurate tracking results in brain tumour patients.

The objective of this study, therefore, was to compare the use of pontine and/or internal capsule ROIs in addition to an nTMS-defined cortical seed ROI for anatomical plausibility of fibre reconstruction. Moreover, we tested for the influence of factors such as oedema on the quality and, thus, plausibility of the nTMS- and DTI-based tractography in brain tumour patients. We hypothesized that, due to tumour-induced brain shift and perifocal oedema, the ROI location in the internal capsule would result in less plausible fibre tracts compared to pontine regions. Moreover, we reasoned that high FA values were associated with better tractography results since the parameter reflects directionality of the fibres derived from the DTI data.

2. Material and methods

2.1. Patients

Thirty-two patients undergoing brain surgery because of intracranial tumours adjacent to or involving the precentral gyrus — representing M1 — and/or the CST were prospectively recruited in 2012 and 2013 and investigated by nTMS and DTI-based tractography of the CST prior to surgery. All patients were treated in the Department of Neurosurgery, Cologne University Hospital/Germany. The study was approved by the local ethics committee of the Medical Faculty of the University of Cologne. The tumour entities consisted mostly of primary brain tumours ($n = 22$) and carcinoma metastases ($n = 6$) (Table 1). All patients were able to care for themselves (Karnofsky performance scale (KPS; Karnofsky and Burchenal, 1994) >70%) and were eligible for MRI.

2.2. MRI and DTI acquisition

All measurements were performed on a 3 T MR scanner (MAGNETOM Trio, Siemens Healthcare, Erlangen, Germany) equipped with gradients of maximum strength of 40 mT/m per axis. A birdcage coil was used for radiofrequency transmission and an 8-element receiver coil for signal detection. Data quality was examined by acquiring a single $b = 0$ DWI scan — that is, no diffusion weighting — and inspecting it for artefacts. The parameters of the DTI acquisition were: repetition time (TR) = 7000 ms, flip angle = 90°, field-of-view (FOV) = 224×166 mm^2, slice thickness 2 mm, interleaved acquisition, no gap; matrix size = 112×112; phase resolution 75%; 60 slices; bandwidth (BW) = 2350 Hz/px; echo time (TE) = 81 ms; acceleration factor for parallel imaging (iPAT) = 2. Further parameters specific to the DTI acquisition were: diffusion weighting $b = 800$ s/mm^2; 30 directions; one $b = 0$ acquisition; 2 repetitions. The total acquisition time of the DTI measurement was 7:20 min.

The MR protocol included the following sequences: MP-RAGE (T1-weighted) before and after gadolinium (Gd) contrast agent, SPACE (T2-weighted) and FLAIR. The total acquisition time for the MR measurements was less than 1 h.

2.3. nTMS

All patients had a clear surgical indication for brain surgery, and hence non-invasive mapping of the operation field using nTMS was performed in all patients in the case of the absence of absolute TMS contraindications such as metal implants. However, in this cohort of patients, epilepsy was not considered a contraindication for single pulse nTMS as long as all patients were under effective anticonvulsive treatment and did not show epileptic potentials as revealed by encephalography

Table 1
Distribution of tumour entities within trial subjects. The histological analysis of most recruited patients revealed primary brain tumours ($n = 22$), followed by carcinoma metastasis ($n = 6$).

Oligo-/astrocytoma		22
	Glioblastoma	15
	Astrocytoma WHO III°	3
	Astrocytoma WHO II°	1
	Oligodendroglioma WHO II°	3
Other tumour entities		10
	Carcinoma metastasis	6
	Meningioma	3
	B-cell-lymphoma	1

(EEG). As such, the risk of inducing a seizure was very low, and was clearly outweighed by the benefit of gathering information about eloquent cortical sites in order to prevent operation-induced motor disability. The patient population included patients ($N = 17$) with known epilepsy all of whom were treated with levetiracetame ($N = 13$) or other anticonvulsive drugs ($N = 4$). In none of these patients a seizure occured during or after administration of single pulse nTMS.

Neuronavigated TMS was conducted using the eXimia NBS system (version 4.2, Nexstim Ltd., Helsinki, Finland) and a figure-of-eight-shaped stimulation coil. Subjects were comfortably seated in an adjustable armchair with a headrest. For head tracking, we used the standard tracking unit which was fixed to the subjects' front using an elastic band and additional tape. The head of the subject was co-registered with the corresponding high-resolution anatomical MR image acquired from each subject as described above. Coregistration was achieved using three main anatomical landmarks (nasion, crus helicis of each ear) and nine additional points along the whole extent of the skull. This procedure yields a co-registration error of less than 2 mm (root mean square difference between the coregistered anatomical landmarks estimated by the neuronavigation software). Whenever clinically meaningful, i.e. whenever the respective body part representation or associated CST fibres were adjacent to the tumour, motor evoked potentials (MEPs) were recorded using surface electrodes (Ambu Neuroline, Bad Nauheim, Germany) mounted above the abductor pollicis brevis muscle (APB), the plantar muscle (PM) and the anterior lateral tongue muscles (LT) (Weiss et al., 2013). The choice of one target muscle each per body part representation was based on the fact that even if more muscles per body part representation were used, the results are very likely to be extremely similar given the millimeter range distance of neighboured muscles in M1 (Bashir et al., 2013) and the spatial smoothness of the DTI data within the same range. To avoid false-positive registration of nTMS-induced MEPs (e.g., due to direct stimulation of the facial nerve), we only accepted latencies within the following ranges for the respective group of muscles: 17–30 ms for APB, 31–60 ms for PM, and 9–16 ms for LT (Rödel et al., 1999, 2001, 2003; Saisanen et al., 2008; Weiss et al., 2013). As an intra-individual condition, data were additionally acquired from the hand representation (APB) of the unaffected hemisphere which served as an intra-individual control.

Stimulation intensity was adjusted to 110% of the resting motor threshold (RMT) of the respective muscle which was determined at the estimated "hot spot" of the respective body part representation. The anatomical position of the hot spot was established by performing a coarse mapping around the anatomical landmarks of the respective motor cortex representation area (Penfield and Rasmussen, 1950; Weiss et al., 2013): (i) the "hand knob formation" (Yousry et al., 1997) for ABP mapping, (ii) the cortex close to the interhemispheric fissure for foot representation mapping, and (iii) the frontal operculum for the lips and tongue area. The RMT was defined as the minimum stimulus intensity capable of inducing MEPs greater than 50 μV peak-to-peak amplitude in at least 5 out of 10 consecutive trials in the estimated 'hot spot' of the relaxed muscle (Rossini et al., 1994; Julkunen et al., 2009; Weiss et al., 2013): The hot spot was defined as the cortical stimulation site at which coil positioning, orientation and tilt yielded the highest MEP amplitude. Whenever involuntary pre-innervation was observed in the EMG traces, stimulation trials were excluded from further analysis. The coil orientation was kept stable (according to its orientation at the hot spot) during the whole mapping procedure. For mapping of the hand and the tongue area, the coil position was usually perpendicular to the course of the central sulcus (posterior–anterior current). For mapping of the foot area, the coil position was perpendicular to the course of the interhemispheric fissure (mediolateral current). For mapping of the tongue area, some nTMS sessions required voluntary pre-innervation to reduce excitability thresholds in order to prevent direct nerve stimulation and/or discomfort. For each muscle representation, 120–200 pulses (depending on the size of the respective representations and subject compliance) were applied using a stimulation grid projected onto the head representation and visualized by the neuronavigation software. The spacing between the grid nodes was 5 mm. Note that for all mappings, coil orientation was independent of the grid. Two to three pulses were applied per stimulation position, i.e., grid square unit. The outer margin of a given functional area was determined by two adjacent negative spots, i.e., the position where no MEP could be elicited in at least consecutive stimulation trials (Weiss et al., 2013). Before exporting the acquired data in a series of binarized DICOM images, all positive EMG responses underwent manual selection with regard to the effects of potential involuntary preinnervation and to eliminate false-positive results. Thereafter, the cortical representation of the hot spot of each body part representation was exported.

2.4. Tractography

The results of the nTMS experiments, i.e., the binarized DICOM series displaying the cortical representation of the respective M1 hot spot as well as the anatomical MRI and eddy-current-corrected DTI sequences were imported into the tracking software (Brainlab iPlan 3.0.0, Heimstetten, Germany). Tracking was performed using a deterministic fibre tracking algorithm which integrates voxel-wise diffusion properties for fibre assignment by continuous tracking (FACT) (Mori et al., 2002).

2.5. Definition of seeding ROIs

2.5.1. Neuronavigated-TMS defined cortical M1 ROI

First, to define the cortical ROI from the nTMS, the nTMS-derived DICOM series were co-registered with the anatomical MR image which had been used for the nTMS examination (usually T1 w/o Gd-enhancement). Thereafter, the respective T1 sequence was co-registered with further anatomical sequences (T2, FLAIR) and the $b = 0$ dataset of the DTI time-series. Fusion accuracy with nTMS data were checked by comparison of the respective coordinates in the visualization software and in the raw data. The fusion-associated mismatch was <2 mm in all subjects. Hot spots were labelled as ROIs and enlarged by 2–3 mm, according to the estimated registration and fusion mismatch, so that the volumes of the resulting spheric cortical ROIs representing the M1 hot spots were standardized to a total volume of 0.9 ± 0.1 cm^3 (Fig. 1A). Moreover, to check for the reproducibility of the results using the entire M1 map of a given body part as starting point for tractography, we computed for all patients an additional analysis based on all stimulation points of the hand representation area with MEP potentials >50 μV. Data were identically processed as the hot-spot tracking data.

2.5.2. Subcortical ROIs

According to anatomical considerations concerning the course of the CST and with regard to the ROI locations typically reported in the literature, a cubic box was inserted to define further ROIs (i) in the region of the posterior limb of the internal capsule (PLIC; Han et al., 2010) and (ii) at the anterior inferior pontine level (aiP; Seo et al., 2013). In order to standardize ROI positioning, PLIC ROIs were set on the level of the interventricular foramina of Monro which serves as a well-defined anatomical landmark. The aiP-ROI, whenever possible due to the FoV, was inserted caudally from the upper and middle cerebellar peduncle (Fig. 1A).

2.6. Fibre tracking parameters

All fibres were calculated originating from the nTMS-defined cortical hot spot ROIs (CoHS) and passed through either one or both of the above-mentioned cubic boxes, such as: (a) CoHS–PLIC, (b) CoHS–aiP, (c) CoHS–PLIC–aiP. Vector step length was 1.6 mm and the angular threshold was 30°. The minimal fibre track length (MFL) was not pre-

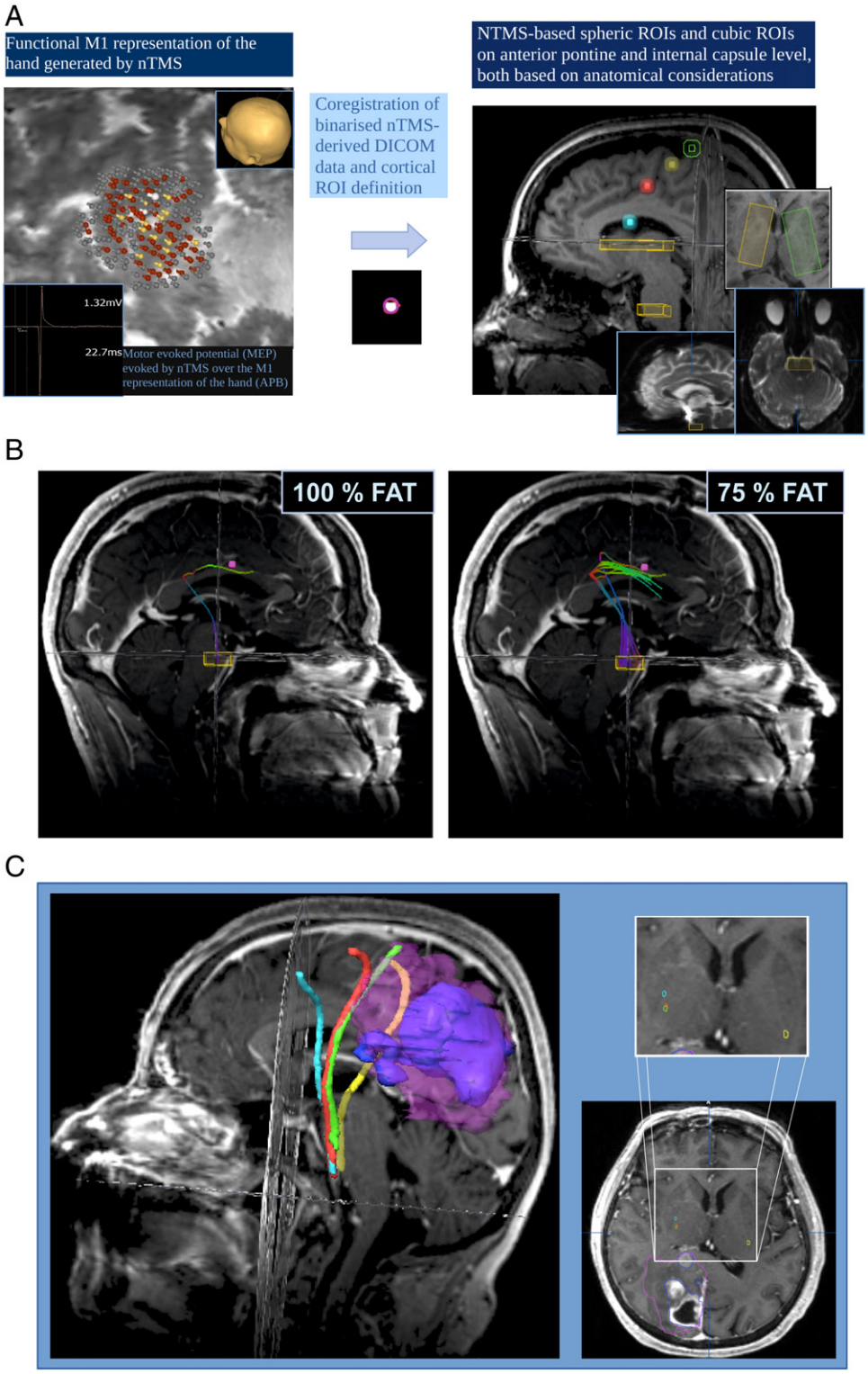

Fig. 1. Illustrative overview of tractography technique. (A) Definition of the cortical ROI (CoHS) and the cubic ROI on pontine level (aiP). After nTMS mapping (left) and determination of the MEP hot spot the respective cortical M1 representation (e.g., hand) was exported as binarized DICOM data. Then, tractography was performed as follows: (i) The binarized DICOM datasets displaying the cortical M1 hot spot (CoHS) of the body part of interest which resulted from nTMS mapping (left) are integrated into the iPlan software. (ii) The CoHS — here outlined in violet — (middle) are labelled manually and the ROI are enlarged by 2–3 mm in order to achieve a standardized ROI volume of 0.9 ± 0.1 cm^3. Afterwards (iii), the cubic ROI boxes are set in the region of the anterior inferior pons (aiP; right) and in the area of the genu and the posterior limb of the internal capsule (IC; lower right), hereby using the DTI (B0) sequence to control for FOV and artefacts. (B) CST fibres tracked from the cortical M1 hot spot (CoHS) of the tongue: comparison of FA-dependent methods. For further analysis, the most specific approach, i.e., evaluating the course of the minimal acquirable fibre (i.e., 100 % FAT, left) was chosen. Here, the approach is compared to the more sensitive tracking approach setting the FA value at 75 % of the FAT (right; according to Frey et al., 2012). (C) CST fibres originating from the cortical M1 hot spots of different body part representations, located anteriorly to the tumour bulk. Left: function-associated fibre tracts were generated using the cortical spheric ROI based on nTMS results and a cubic pontine ROI set according to anatomical knowledge (see panels A and B). Direction-encoded tracts were transformed into fibre objects outlined in distinct colours (yellow: contralesional hand, green: ipsilesional foot, red: ipsilesional hand, light blue: ipsilesional tongue). Right: the results show a plausible course of the distinct fibre tracts according to anatomical considerations. e.g., all tracts *pass* through the posterior limb of the internal capsule (contrast-enhancing tumour bulk outlined in dark blue, perilesional oedema displayed in violet), hereby respecting the somatotopic organization within the internal capsule with the tongue-associated tracts (light blue) located anteriorly to the hand- (red) and the foot-associated tracts (green) (Park et al., 2008, Pan et al., 2012).

set in this multiple-ROI tracking approach and, thus, set at the minimum allowed by the software of MFL = 1. To compute the fractional anisotropy threshold (FAT) (Frey et al., 2012), the FA value was gradually increased or decreased until the highest FA value was identified which resulted in at least one reconstructed fibre. This value was defined as 100% FAT and the resulting fibres were used for the analyses. Other authors have proposed to use lower values such as 75% FAT to increase sensitivity with respect to surgery (Frey et al., 2012). In this study, the minimal computable fibre tract defined by tracking at 100% FAT was used for the analysis in order to minimize the number of false-negative tracts and to facilitate the interpretation of the fibre course (Fig. 1B, C). However, to investigate the impact of the relative FA value chosen for tractography (100 % vs. 75% of the FAT) on the fibre tracking plausibility, we additionally computed fibre tracts at 75% FAT using identical tracking conditions compared to the 100% FAT approach in a representative data subset, i.e., tracts originating from the M1 representation of the ipsilesional hand.

2.7. Data analysis

2.7.1. Volumetry

Volumetry of (i) contrast-enhanced (CE) T1 tumour volume and (ii) the volume of T2-hyperintense tumour areas, representative for tumour oedema, was performed PC-based using iPlan (Brainlab iPlan 3.0.0, Heimstetten, Germany). The software enables the observer to switch between cross-sectional views in any plane (axial, sagittal, coronal) as well as labelling of the respective tumour areas.

2.7.2. Plausibility ratings

All fibre tracts (contralesional hand, ipsilesional: hand, foot, tongue) — each in the following three ROI conditions a, b and c — were analysed separately by two independent blinded observers, i.e., a neuroradiologist and a neurosurgeon, in 3D. The courses of the fibre tracts for the tracking conditions (a) CoHS–PLIC, (b) CoHS–aiP, (c) CoHS–PLIC–aiP were checked for fibre course plausibility in a dichotomic manner (i.e., yes/no) by the two investigators. Both investigators were familiar with the anatomical course of the CST and its correlates in cross-sectional MR images. The following anatomical constraints were applied: (i) Aberrant fibres such as fibres crossing to the contralateral hemisphere, passing through the anterior frontal, temporal, parietal or occipital lobe were classified non-plausible. (ii) Corticonuclear fibres originating from the hand or the foot M1 representation which terminated within the cerebellum and/or passed through the cerebellar peduncles and did not continue along the expected CST course were considered non-plausible. Moreover, corticobulbar fibres originating from the tongue representation were only considered plausible if they passed through the anterior part of the cerebral peduncle on the midbrain level. (iii) Fibres missing the posterior limb or the genu of the internal capsule were regarded non-plausible in the CoHS–aiP condition (b). By contrast, for condition (a) — CoHS–PLIC tracking - fibre courses were only considered as plausible if they were passing through the cerebral peduncles, i.e., anterior to the substantia nigra and through the anterior portion of the pons. Plausibility analysis was performed PC-based using iPlan (Brainlab iPlan 3.0.0, Heimstetten, Germany). The software enables the observer to switch between cross-sectional views in any plane (axial, sagittal, coronal) as well as to reconstruct the fibre tracts in 3D. All fibre tracts (contralesional hand, ipsilesional: hand, foot, tongue; each in ROI conditions a, *b* and c) were analysed separately by each of the independent observers.

2.7.3. Interrater reliability

To test for the inter-rater reliability for the two raters as well as to estimate the agreement between methods (subcortical ROI positioning), Cohen's Kappa was calculated using the R software package (version 3.0.2, "cohen.kappa"-function, "psych"-package; R Core Team 2013; http://www.R-project.org/).

2.7.4. Influence of subcortical ROI position on fibre course plausibility

McNemar's chi-squared test for independence was used to test the influence of the two different cubic ROI locations on plausibility ratings within the same group of patients (McNemar and Quinn, 1947) using the R software package. Moreover, Odd's Ratio (OR) was calculated following the formula: $OR = (n_{11} \times n_{22})/(n_{12} \times n_{21})$. The level of confidence was defined at 95% (i.e., $p < 0.05$). The analysis was additionally performed using the entire M1 map of the ipsilateral hand representation as a starting ROI for tractography (instead of the hot spot) in order to check the robustness of the results under more clinically usual tracking conditions.

2.7.5. Influence of clinical cofactors on fibre course plausibility ratings

In addition to the DTI parameters, the following parameters were tested for the influence on plausible versus non-plausible fibre tracts: RMT, FAT, MFL, tumour volume, oedema volume, presence of oedema within the PLIC (dichotomous, i.e., yes/no), the histological tumour entity (intrinsic vs. non-intrinsic, glioblastoma vs. others) and the KPS score. Differences between plausible vs. non-plausible fibre tracts in oedema volume and tumour volume were analysed using ANOVA, such between plausible vs. non-plausible tracts in the KPS score and in RMT were calculated using non-parametric tests (Mann–Whitney-U), depending on the distribution of the co-factors. The influence of oedema within the internal capsule (i.e., present vs. non-present) and the tumour type on the fibre course plausibility ratings were assessed by Pearson's Chi-Square Test. Correlations between potential influencing factors with the plausibility ratings were calculated using point-biserial correlation (Pearson's product moment correlation). Additional linear discriminant analysis was performed to test for the predictive value of variables on fibre tract.

2.7.6. Correlation between tractography parameters and plausibility

Correlations between the variables FAT and MFL with the dichotomous outcome variable, i.e., the plausibility of the CST fibre course, were calculated using Pearson's product moment. To control for the influence of inter-correlated variables, partial correlations were calculated.

2.7.7. Linear discriminant analysis

In addition to the tests outlined above, linear discriminant analysis was performed to test for the predictive value of the different variables on the respective fibre tract plausibility ratings. A Kernel density plot was used for the visualization of the cut-off between plausible and non-plausible fibre tracts depending on either FAT or MFL values. The cut-off values — representing an optimal, linear combination of sensitivity and specificity of prediction — were determined by a receiver operating characteristics (ROC) analysis and were sorted by the maximum value resulting from the formula: "sensitivity" − (1 − "specificity") (Greiner et al., 2000; Hajian-Tilaki et al., 2013) (PASW Statistics 18.0, SPSS Inc., Chicago, IL, USA). Moreover, the precision (i.e., true positives)–recall (i.e., false negatives) cut-even point, i.e., the cut-off where precision and recall are equal were calculated and density distributions were plotted using histograms and Kernel's density curves and by grouped scatter plots.

3. Results

3.1. Patients and descriptive analysis

Thirty-two patients (21 male) with intracranial tumours, in most cases glioblastomas (Table 1) participated in the study. All patients were still in a rather good clinical state as indicated by the Karnofsky Performance Scale (KPS = 90.1 ± SD 8.0). The mean tumour volume was 20.8 ± SD 17.9 cm^3 and the mean oedema volume was 56.2 ± SD 35.5 cm^3. The tumour location (according to the CE-T1 scans) was as follows: precentral (CoHS and fibre tracts posterior to the tumour) 31.7%,

central (CoHS and/or minimal computable fibre tracts overlapping with tumour volume) 31.7%, and postcentral (CoHS and fibre tracts anterior to the tumour) 36.6%. In 6/32 patients T2 MRI revealed oedema within the PLIC. None of the patients showed signs of oedema in the aiP. 17/32 patients had symptomatic epileptic seizures and were treated by anticonvulsive drugs, mostly with levetiracetame ($N = 13/17$). Most patients (25/32) were under anti-oedematous steroid medication at the time of nTMS.

A total of 118 M1 representation areas were mapped by nTMS, i.e., $N = 32$ contralesional APB, $N = 32$ ipsilesional APB, $N = 28$ ipsilesional LT, and $N = 26$ ipsilesional PM. The reasons for incomplete mappings for some body parts was that only those regions were investigated which were adjacent to the tumour regions in order to minimize discomfort for the patients. For example, if the tumour was located in between the hand and the tongue representation, mapping of the foot representation was not performed.

The RMT was 38.8 ± 12.2 maximum stimulator output (MSO) for the contralesional hand (APB), 39.7 ± 12.7 MSO for the ipsilesional hand, 64.1 ± 18.0 MSO for the foot (PM) and 45.3 ± 10.1 MSO for the tongue (LT), respectively. No severe adverse effects were reported, with on 2/32 patients complaining of transient (<24 h) headache following nTMS.

3.2. Plausibility analysis

After DTI preprocessing, three fibre tracts were reconstructed connecting the respective ROI volumes: CoHS–PLIC, CoHS–aiP, and CoHS–PLIC–aiP. The inter-rater reliability of the plausibility analyses was excellent for the CoHS–aiP condition (Cohen's Kappa $k = 0.96$) and very good for the CoHS–PLIC–aiP condition ($k = 0.86$) as well as for the CoHS–PLIC condition ($k = 0.80$; Table 2). Due to the excellent concordance of the independent ratings and to simplify the data presentation, plausibility results reported below are based on the neuroradiologist's rating. The size of the cubic ROIs (capsule, pons) and the size of the cortical M1 ROIs — being standardized to 0.9 ± 0.1 cm^3 — was investigated to some extent and found to have no significant impact on the fibre course plausibility results ($p > 0.1$, Bonferroni corrected).

3.2.1. Comparison of subcortical ROI location

The CoHS–aiP algorithm resulted in significantly more plausible fibre tracts as compared to CoHS–PLIC ($x^2_{McNemar} = 67.12$, $p_{McNemar} < 2.55e-16$; OR = 20.0; Table 4A, B and Fig. 2). The result was significant ($p_{McNemar} < 0.001$) for all ipsilesional body parts (Table 3). However, due to data distribution, McNemar's test could not be performed in the contralesional hand condition. The combination of ROIs, i.e., CoHS–PLIC–aiP, did not yield better tracking results, as compared to CoHS–aiP alone ($p_{McNemar} = 1$). The convergence between both these approaches was high (Cohen's Kappa $k = 0.83$; Table 2). This result remained significant using 75% of the FAT value ($p_{McNemar} = 0.02$; Supplementary Table S1) as well as using the entire M1 map instead of the hot spot ($p_{McNemar} = 0.003$; Supplementary Table S2) as a starting ROI for tractography in a representative subset of fibres originating from the ipsilesional hand representation despite a generally higher number of aberrant fibre tracts for both subcortical ROI conditions.

3.2.2. Influence of CoHS body part assignment on fibre course plausibility

Hand fibre tracts on the healthy brain side showed best plausibility results when using the CoHS–aiP or the combined CoHS–PLIC–aiP tracking method (100 % plausibility), followed by the ipsilesional CS fibre tracts originating from the CoHS of the hand (94%), the foot (81% [CoHS–aiP]/88% [CoHS–PLIC–aiP]); the tongue (79% [CoHS–aiP]/68% [CoHS–PLIC–aiP]) showed the worst plausibility results. The data acquired by the CoHS–PLIC tracking method showed a similar effect of body part representation area, with much lower plausibility rates, however (contralesional hand: 34 %, ipsilesional hand: 53 %, foot 12 %, tongue 11 %; Table 4A, B and Fig. 2).

3.3. Factors influencing the tracking results

Since the data demonstrated that positioning of the subcortical ROI in the pontine area (aiP) leads to best tractography results, as compared to the internal capsule (PLIC), multivariate analysis was restricted to the data subset comprising the "CoHS–aiP" tractography condition.

3.3.1. Influence of clinical cofactors on fibre course plausibility

The presence of oedema within the PLIC was associated with less plausible tractography data ($p_{xsq} = .007$ with X-Sq = 7.27; OR = .143; Table 5 and Supplementary Fig. S1). The influence of the oedema involving the internal capsule on CST plausibility was most evident for the MCT fibres originating from the hand CoHS and the foot CoHS ($p < .05$, Bonferroni corrected). However, the influence of internal capsule oedema on tongue-derived CS fibres did not meet statistical significance (Table 5). In contrast to the influence of oedema, the tumour histology itself (intrinsic brain tumours/malignant brain tumours/glioblastomas vs. others) had no significant influence on the plausibility results ($p_{xsq} > 0.1$). Other variables such as the KPS, the RMT, the T1-CE tumour volume and the overall T2 oedema showed neither a significant

Table 2
Interrater reliability. The plausibility ratings regarding the corticospinal fibre tracts of two independent, blinded investigators, i.e., a neurosurgeon and a neuroradiologist were compared. The rating of the fibre tracts was based on anatomical knowledge (see Material and methods section). The consensus between the two independent raters was excellent, especially for the CoHS–aiP tracking condition ($k = 0.96$; highlighted in bold). Moreover, the agreement between two tracking conditions involving (i) only the pons as subcortical ROI or (ii) pons and internal capsule as subcortical ROIs, i.e., CoHS–aiP and CoHS–IC–aiP, was good (neurosurgeon's analysis: $k = 0.62$; neuroradiologist's analysis: $k = 0.83$).

Interrater reliability (Cohen's kappa)			
Agreement on fibre tract plausibility between raters. Neurosurgeon (NS) vs. neuroradiologist (NR)			
	Subcortical ROI location	Kappa value	Confidence interval
	Pons (aiP)	**0.96**	**0.87–1.0**
	Internal capsule (IC)	0.80	0.68–0.92
	Both (aiP–IC)	0.86	0.72–1.0
Agreement on fibre tract plausibility between tracking methods. Subcortical ROI location: pons (aiP) vs. internal capsule (IC) vs. both (IC–aiP)			
Rater	ROI locations compared	Kappa value	Confidence interval
NS	aiP–IC	0.1	0.04–0.16
	aiP–IC–aiP	**0.62**	**0.44–0.81**
	IC–IC–aiP	0.07	0.03–0.11
NR	aiP– IC	0.07	0.01–0.13
	aiP–IC–aiP	**0.83**	**0.66–0.99**
	IC–IC–aiP	0.10	0.04–0.15

Table 3
Effect of subcortical ROI location on plausibility of distinct M1-derived fibre tracts. The CoHS–aiP algorithm resulted in significantly more plausible fibre tracts as compared to CoHS–PLIC for all ipsilesional body parts. However, due to the data distribution, McNemar's test could not be performed in the contralesional hand condition. The results are displayed in a bar plot in Fig. 2B.

CoHS (M1)	CoHS–aiP fibre tract plausibility	CoHS–IC fibre tract plausibility		χ^2	$p_{McNemar}$
		No	Yes		
Hand (APB) contrales	No	0	0	n.a.	n.a.
	Yes	21	11		
Hand (APB) ipsilesional	No	2	0	11.08	0.0008
	Yes	13	17		
Foot (PM) ipsilesional	No	4	1	14.45	0.0001
	Yes	19	2		
Tongue (LT) ipsilesional	No	6	0	17.05	0.0000
	Yes	19	3		
Total (all CoHS/M1)	No	12	1	67.12	0.0000
	Yes	72	33		

Table 4
Tables A and B and Fig. 2: Cubic ROI on pontine level (aiP) allows generation of more plausible CS fibre tracts, compared to cubic ROI defined by posterior limb of the internal capsule (IC). Applying the CoHS–aiP algorithm resulted in significantly more plausible fibre tracts, as compared to CoHS–IC (Pearson's X-squared = 85.7673, $p < 2.2e{-}16$; Table A and Fig. 2; fig: bars labelled in red). The combination of ROIs, i.e., CoHS–IC–aiP, almost never contributed to more plausible results, as compared to CoHS–aiP alone ($p = 1$). For better overview, please concern summary Table B.

(A) Plausibility of corticospinal tract depending on region of interest (ROI) — location in percent data grouped by M1 CoHS

Muscle		APB contralateral		APB ipsilateral		PM ipsilateral		LT ipsilateral	
Algorithm		Count	Percentage	Count	Percentage	Count	Percentage	Count	Percentage
Pons (CoHS-aiP)	Plausible tract	32	100 %	30	94 %	21	81 %	22	79 %
	Non-plausible	0	0 %	2	6 %	5	19 %	6	21 %
	No tract	0	0 %	0	0 %	0	0 %	0	0 %
	Total	32	100 %	32	100 %	26	100 %	28	100 %
Internal capsule (CoHS–IC)	Plausible tract	11	34 %	17	53 %	3	12 %	3	11 %
	Non-plausible	21	66 %	15	47 %	23	88 %	25	89 %
	No tract	0	0 %	0	0 %	0	0 %	0	0 %
	Total	32	100 %	32	100 %	26	100 %	28	100 %
Combined ROIs (CoHS–IC–aiP)	Plausible tract	32	100 %	30	94 %	23	88 %	19	68 %[a]
	Non plausible	0	0 %	2	6 %	3	12 %	4	14 %
	No tract	0	0 %	0	0 %	0	0 %	5	18 %
	Total	32	100 %	32	100 %	26	100 %	28	100 %
Total	Plausible tract	75	78 %	77	80 %	47	60 %	44	52 %
	Non plausible	21	22 %	19	20 %	31	40 %	35	42 %
	No tract	0	0 %	0	0 %	0	0 %	5	6 %
	Total	96	100 %	96	100 %	78	100 %	84	100 %

(B) Plausibility of corticospinal tract depending on region of interest (ROI) Summary table

Algorithm	Pons (CoHS–aiP)		Internal capsule (CoHS–IC)		Combined ROIs (CoHS–IC–aiP)		Total	
	Count	Percentage	Count	Percentage	Count	Percentage	Count	Percentage
Plausible tract	105	89 %	34	29 %	104	88 %	243	69 %
Non-plausible / no tract	13	11 %	84	71 %	14[b]	12 %	111	31 %
Total	118	100 %	118	100 %	118	100 %	354	100 %

[a] 83% of tracts, $n = 5$ no tract.
[b] Including $n = 5$ w/o tract (generation not possible).

correlation with fibre course plausibility (point-biserial correlation coefficient at least $R^2 < .02$, $p > 0.1$) nor a relevant influence on the outcome variable, i.e., plausibility of the CS fibre course as revealed by linear discriminant analysis.

3.3.2. Influence of FAT and MFL values on plausibility of CS fibre tracts

Both FAT and the MFL significantly influenced the plausibility of the computed CS fibre tracts. Low FAT values were associated with a lower number of plausible tracts for all of the tracking methods. The mean FAT

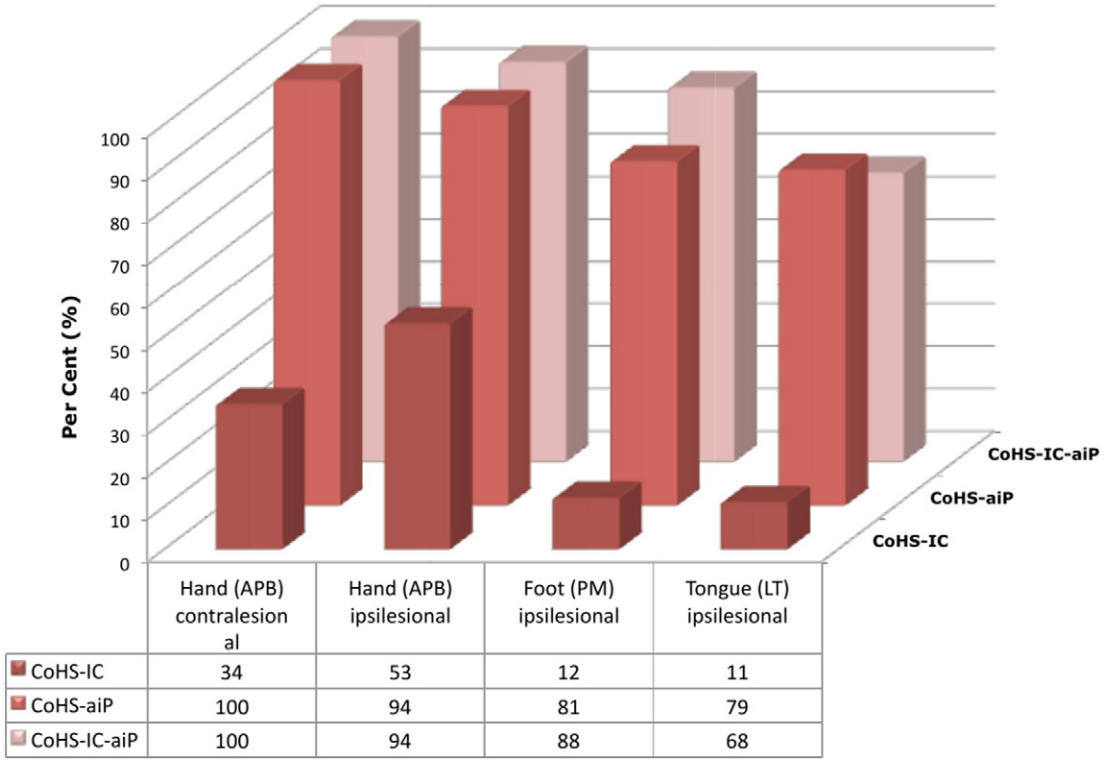

Fig. 2. Plausibility of the corticospinal tract depending on region of interest (ROI)-location.

Table 5
Plausibility of fibre courses, grouped by presence of oedema within the IC (columns), *overall and* distinguished by body-part affiliation of the respective CS fibre tracts (rows). In the presence of IC-oedema the rate of plausible tracking results was decreased from 93 % to 65 % ($p_{xsq} = 0.007$). The effect of the oedema was most evident for the somatotopic fibre tracts originating from the M1 representation of the hand.

Plausibility of fibre courses, *overall and* grouped by presence/absence of oedema within the internal capsule (IC) and by the M1 representation of fibre origin (CoHS)

				Fibre course plausibility		Total	p_{xsq}
				No	Yes		
All fibres	IC oedema	Absent	Count	5	64	69	.007
			% of total	6 %	74 %	80 %	
		Present	Count	6	11	17	
			% of Total	7 %	13 %	20 %	
	Total		Count	11	75	86	.002
			% of total	13 %	87 %	100 %	
Hand (APB)	IC oedema	Absent	Count	0	26	26	
			% of total	0 %	81 %	81 %	
		Present	Count	2	4	6	
			% of total	6 %	13 %	19 %	
	Total		Count	2	30	32	
			% of Total	6 %	94 %	100 %	
Foot (PM)	IC oedema	Absent	Count	1	20	21	.027
			% of Total	4 %	77 %	81 %	
		Present	Count	2	3	5	
			% of Total	8 %	11.5 %	19 %	
	Total		Count	3	23	26	
			% of Total	11.5 %	88.5 %	100.00%	
Tongue (LT)	IC oedema	Absent	Count	4	18	22	.423
			% of total	14 %	64.5 %	79 %	
		Present	Count	2	4	6	
			% of total	7 %	14.5 %	21 %	
	Total		Count	6	22	28	
			% of total	21 %	79 %	100 %	

values of plausible CS fibres were significantly higher (mean [CoHS–aiP] = 0.23 ± 0.06) than those FAT values of the non-plausible group (mean [CoHS–aiP] = 0.076 ± 0.09; $p < 0.001$). This finding was significant for any of the ROI-dependent tracking methods (CoHS–PLIC: $p = .005$; CoHS–PLIC–aiP: $p = .003$; Fig. 3). Point-biserial correlation analysis revealed a strong positive correlation between the FAT values and the dichotomous outcome measure, i.e., fibre tract plausibility (Table 6). However, both variables show a significant negative correlation (Pearson correlation: $R^2 = 0.304$, $p < 0.001$; Table 6 and Fig. 4B). Controlling for the influence of MFL, the partial correlation of FAT with fibre course plausibility was still significant for each subgroup analysis (Table 6). Comparison of means revealed significantly higher values of the minimal fibre length (MFL) in the subgroup with non-plausible fibre tracts compared to those patients with plausible fibre tracts (mean [CoHS–aiP; plausible] = 101.1 ± 14.5, mean [CoHS–aiP; non-plausible] = 120.9 ± 17.9; CoHS–aiP: $p = .001$; CoHS–PLIC–aiP: $p = .001$; Fig. 3).

Point-biserial correlation analysis revealed a rather strong negative correlation of the MFL results with the plausibility of the CST course (Table 6). However, this correlation did not survive partial correlation, controlled for the influence of the FAT on the fibre course plausibility (Table 6).

3.3.3. Predictive value of FAT and MFL for fibre tract plausibility and cut-off values

Linear discriminant analysis confirmed the correlation and predictive potential of both variables with regard to plausibility prediction (coefficients of linear discriminants [cld]: cld[FAT] = 8.95, cld [MFL] = −.024). Dependent on case classification (plausible/non-plausible), a distinct data distribution can be observed in a FAT (*x*-axis)- and MFL (*y*-axis)-based scatter plot (Fig. 4B). Cut-off values were calculated for each tracking condition by ROC analysis (FAT — fibre course plausibility: cut-off = 0.105; MFL — fibre course plausibility: cut-off = 121.5 mm; Table 7 and Fig. 4A, B).

4. Discussion

4.1. General considerations and side effects

A number of studies have investigated tractography-guided brain tumour surgery over the past years and reported good clinical results (Wu et al., 2007) as well as convergence between intraoperative direct subcortical stimulation (DsCS) and preoperative DTI-tracking data (Prabhu et al., 2011; Ohue et al., 2012; Zhu et al., 2012; Vassal et al., 2013). However, conclusions to be drawn from intraoperative DsCS concerning the accuracy of DTI-based tractography are strongly limited by the brain shift that inevitably occurs to a certain extent during surgery (Romano et al., 2011). Furthermore, there is little agreement concerning the underlying tracking algorithms such as the location of subcortical ROIs: Mostly, the posterior limb of the internal capsule (D'Andrea et al., 2012; Frey et al., 2012) and/or the anterior pons/cerebral peduncle (Frey et al., 2012; Ohue et al., 2012; Bucci et al., 2013; Mandelli et al., 2014) are used. There is increasing evidence that probabilistic fibre tracking provides more accurate fibre tracking results compared to deterministic tracking (Bucci et al., 2013; Mandelli et al., 2014).

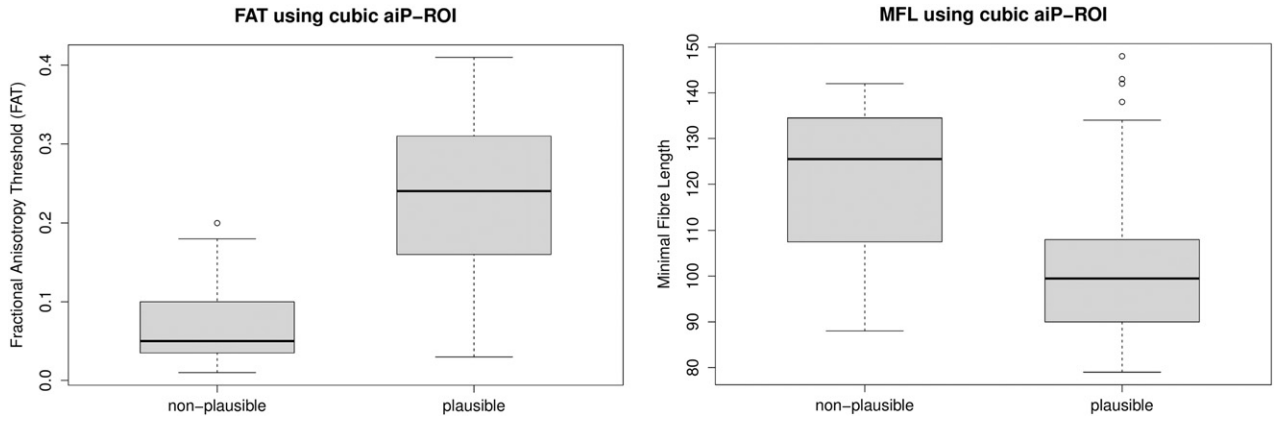

Fig. 3. Low fractional anisotropy thresholds (FAT) and minimal fibre length (MFL) correlate with poor plausibility of CS fibre tracts. Left: the FAT is an indirect measure for the directionality of diffusion and, thus, of the likelihood to detect subcortical fibre tracts by DTI processing. As expected, significantly higher FAT values were encountered within the patient subset with plausible CST fibre course results compared to the non-plausible CST group ($p_{mwu} = .000$). A significant point-biserial correlation was found between FAT values and fibre course plausibility for all body part associations (**; Table 6). Right: the MLF reflects the course of the corticospinal fibres connecting the standardized ROIs (CoHS, aiP). Comparison of means revealed a significant difference between the subset of patients with plausible CST fibre courses compared to those with non-plausible tracts ($p_{mwu} = .001$). The length of the fibres originating from the cortical M1 hot spot of the hand representation was shown to correlate significantly with the anatomical plausibility of their courses (*; Table 6).

Table 6
Correlations between fractional anisotropy threshold (FAT) and minimal fibre length (MFL) with dichotomous outcome variable, i.e., fibre course plausibility. Both FAT and MFL strongly correlate with the outcome parameter "fibre course plausibility". However, both parameters also correlate strongly with each other. The correlation results of the partial correlation analysis (cells faded in grey), controlling for the effect of FAT on the correlation between MFL and CST plausibility, did not meet statistical significance. By contrast, the partial correlation of FAT with fibre course plausibility, controlled for MFL (not shown in table), remained significant (all fibres: $R^2 = .52^{****}$, $p = 2.8e-9$; hand: $R^2 = .37^{*}$, $p = 0.038$; foot: $R^2 = .43^{*}$, $p = 0.031$; tongue: $R^2 = .52^{**}$, $p = 0.006$).

	CST plausibility		MFL	
	R² [conf. interval] point–biserial	p	R² [conf. interval] pearson	p
FAT				
All fibres	.54 [.36 – .63] ****	6.2 e–9	–.55 [–.67 – –.41] ****	9.52 e–11
Hand	.49 [.17 – .72] **	0.0043	–.59 [–.78 – –.31] ***	0.0003
Foot	.55 [.21 – .77] **	0.0015	–.69 [–.85 – –.41] ****	9.29 e–5
Tongue	.57 [.25 – .78] **	0.0036	–.37 [–.65 – .0015] (*)	0.051
MFL			Partial correlation, controlled for FAT	
All fibres	–.38 [–.52 – –.21] **	2.2 e–5	–.142	0.13
Hand	–.35 [–.62 – –.0027] *	0.049	–.085	0.65
Foot	–.38 [–.67 – –.011] (*)	0.057	–.003	0.69
Tongue	–.31 [–.61 – .067]	0.105	–.133	0.51

(*) $p < 0.1$.
* $p < 0.05$.
** $p < 0.01$.
*** $p < 0.001$.
**** $p < 0.0001$.

However, deterministic fibre tracking still represents the most time-efficient and widely distributed method for presurgical fibre course delineation in the neurosurgical field which allows excellent and quick integration with the intraoperative navigation software. Moreover, all previously published data demonstrating the superiority of probabilistic fibre tracking were not based on nTMS-assisted tracking algorithms. Aiming at clinical applicability, we, therefore, based our study on the deterministic fibre tracking approach and compared the two most frequently used ROI positions, i.e. the posterior limb of the internal capsule (PLIC) and the anterior inferior pons (aiP).

To the best of our knowledge, the sample size of 32 patients ranges among the largest studies published on the topic to date. We were able to demonstrate the safety of nTMS and the excellent feasibility of the nTMS-based fibre tracking approach. No severe adverse effects occurred during the examination, e.g., no seizures were evoked by nTMS even though patients with symptomatic epilepsy (under regular anticonvulsive drug treatment) were included into the trial (17/32 patients). This fact confirms the safety of single pulse nTMS (Anand et al., 2002; Tassinari et al., 2003; Rossi et al., 2009). However, 6 % of the patients ($N = 2/32$) complained of transient headaches (<24 h) following nTMS which is a known phenomenon and the most frequent side effect associated with TMS reported with 6–60% for repetitive TMS in the literature (Machii et al., 2006).

4.2. Resting motor threshold

The resting motor threshold (RMT in % of the stimulator output) was 38.8 ± 12.2 % for the contralesional hand (APB), 39.7 ± 12.7 % for the ipsilesional hand, 64.1 ± 18.0 % for the foot (PM) and 45.3 ± 10.1 % for the tongue (LT), respectively. It is a common clinical approach to restrict motor threshold determination to the hand representation and adjust the stimulation intensity of further M1 regions to the respective hand RMT. In this study, the mean foot RMT was 1.61-fold higher than the respective ipsilateral hand RMT and the mean tongue RMT was 1.14-fold increased compared to the hand RMT. However, we observed considerable inter-individual variability of the relationship between hand, foot and tongue RMT and, therefore, do not recommend to adhere to fixed multiplied MT values, relying on the hand RMT but to redetermine the respective RMT for each body part representation, separately. This individual variability of the RMT-ratios between different body part representations may be considerably attributed to anatomical variations such as differences in the coil-to-cortex distance, the thickness of the skull or the cortex at the different stimulation sites (Herbsman et al., 2009; List et al., 2013). However, (i) in order to speed up the RMT determination procedure starting from the estimated RMT and (ii) in case of non-compliance of the patient which can cause the time frame for motor mapping to be quite tight, the use of the above-mentioned percentages (lower extremity: ~160% of hand-RMT, face: ~115% of hand-RMT) can be helpful for RMT estimation. The ratio of 1.61 for the foot/hand RMT ranges within the previously published range (1.6–2.0) for the figure-of-eight shaped coil (Herbsman et al., 2009; Roth et al., 2014). The mean RMT of the tongue (45.3 ± 10.1 %) was consistent with previous reports (Muellbacher et al., 2001).

4.3. Comparison of subcortical ROI locations

In this study, using the anterior pontine region as subcortical ROI (in addition to the nTMS-defined cortical ROI) resulted in significantly more plausible fibre tracts, as compared to the use of the posterior limb of the inner capsule (PLIC) as a subcortical ROI ($p_{McNemar} < 0.001$; Tables 2 and 3). The question of which ROI is most suitable for DTI-based CST reconstruction has recently been addressed by several groups (Koyama et al., 2013; Park et al., 2013), e.g., the high sensitivity of DTI for white matter changes represented by the FA value was shown for the PLIC ROI and a ROI set at the corpus callosum ROI but not for the cerebral peduncle ROI (Koyama et al., 2013). These results may indicate the greater robustness of ROI positioning on the cerebral peduncle or even the pontine region compared to PLIC or corpus callosum which can be regarded as being consistent with our data. Of note, the plausibility ratings based on the aiP ROI were not only superior regarding the ipsilesional hemisphere but also when analysing the corticospinal tract on the contralesional side. Reviewing those cases in more detail, we found that most of the tracts which were considered non-plausible corresponded to thalamocortical fibres, either belonging to the superior

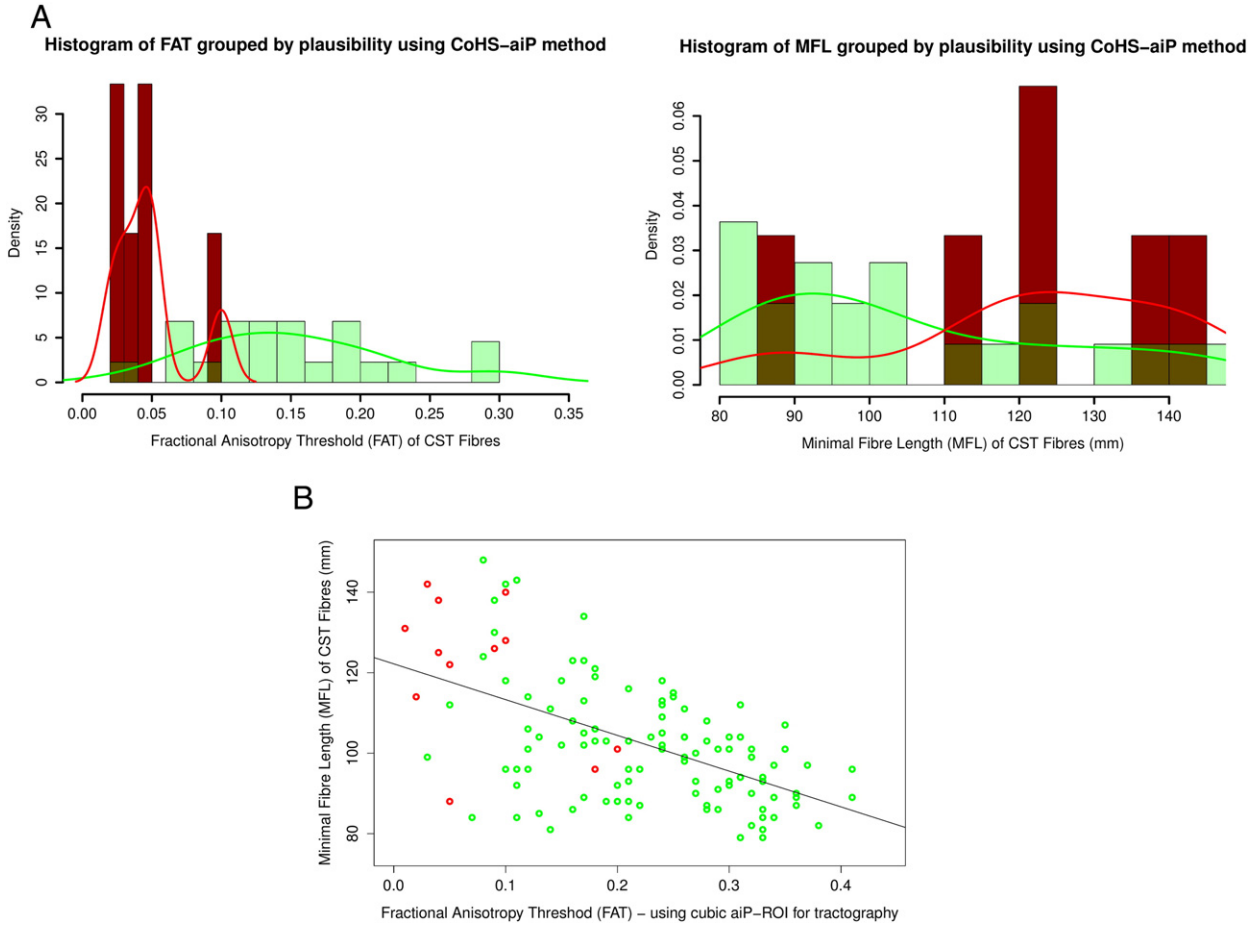

Fig. 4. Distribution and cut off determination of fractional anisotropy threshold (FAT) and minimal fibre length (MFL) values, grouped by their dedicated fibre tract plausibility value. (A) Density distribution of FAT and MFL values, grouped by plausibility of fibre tracts. For better visualization of the FAT (left) and MFL (right) distribution, histograms were generated with overlying Kernel's density curves (cases revealing non-plausible results outlined in dark red, such revealing plausible fibre courses outlined in light green; here shown for the CoHS–aiP tracking algorithm). The graphs show that in cases with low FAT values the likelihood to receive non-plausible or no tracking results at all increases strongly when falling below a value of FAT ≈ 0.10. Accordingly, the probability of non-plausible/no results increases whenever the MFL exceeds length of MFL ≈ 110 mm. (B) Scatter plot of FAT and MFL, grouped by plausibility. The scatter plots shows that non-plausible tracking results occur mostly in case of long MFL and low FAT values (left upper corner; cases with non-plausible/no results represented by red dots; dots representing plausible results outlined in green). The high predictive value of both variables, FAT and MFL, with respect to the group classification "plausible"/"non-plausible" was shown by discriminant analysis. Moreover, a significant correlation between both variables, FAT and MFL, was observed ($p < .01$); the linear regression line is displayed in black ($R^2 = .304$).

thalamic radiation (Cowan and de Vries, 2005) or to sensory pathways, i.e. fibres associated with the spinothalamic tract (Hong et al., 2010a). When setting the subcortical ROI on the aiP level, pure thalamocortical fibres as well as fibres belonging to the spinothalamic system — both located posteriorly to the substantia nigra and posteriorly to the aiP-ROI on the pontine level — were excluded from the tractography results since

Table 7
Cut-off estimation and test statistics. To determine a cut-off value for the FAT and the MLF results, both influencing the outcome of the fibre tracking procedure, i.e., the plausibility of the fibre tracts (binary classifier), a receiver operating characteristic (ROC) curve was generated. The area under the curve (AUC) was calculated and cut-off values were determined (see Material and methods section). The asymptotic p-values (p_a) confirmed the influence of both FAT and MLF on the classifier "plausibility". However, with regard to the influence of the MLF in the CoHS–IC condition only a statistical trend could be observed (values outlined in grey).

		Cut–off	Sensitivity	1 – Specificity	AUC	pa	95% CI	
							Min.	Max.
FAT	CoHS–aiP	.105	.906	.167	.919	.000	.842	.995
	CoHS–IC	.225	.816	.475	.711	.000	.616	.806
	CoHS–IC–aiP	.185	.654	.000	.858	.003	.736	.98
MFL	CoHS–aiP	121.5	.915	.333	.799	.001	.649	.949
	CoHS–IC	103.5	.974	.838	.399	.076	.288	.509
	CoHS–IC–aiP	127.5	.963	.167	.900	.001	.749	.000

they did not pass the aiP-ROI. Thus, anatomical considerations may explain a large proportion of the superiority of aiP-based CS tractography results, even on the contralesional hemisphere.

Moreover, the interesting fact that in three cases with large peritumoural oedema the tongue-derived CS tractography leads to non-plausible results in the CoHS–IC–aiP condition but not in the simpler CoHS–aiP condition recalls the limitations of the FACT tractography approach. In general, the multiple-ROI approach, based on anatomical knowledge, may be advantageous. However, the additional use of large ROIs may as well diminish the advantage of a supposedly highly-precise cortical ROI as – in this study – located by nTMS since when using multiple ROIs the reconstruction results become less dependent on the initial ROI location (Mori and van Zijl, 2002). The multiple-ROI approach may therefore not always be recommendable. However, the number of cases in which CoHS–aiP tractography seemed advantageous compared to CoHS–IC–aiP tractography ($N = 3$) is certainly too low to draw definite conclusions other than pointing out that, due to the mentioned limitations of the tracking algorithms — especially in tissues with an unfavourable signal-to-noise ratio — tractography results should always be interpreted with caution.

4.4. Influence of CoHS body part assignment on fibre course plausibility

Somatotopic tractography and anatomical segregation of different ROIs along the course of the CST have been published by several authors in the past (Park et al., 2008; Yoshiura et al., 2008; Hong et al., 2010b; Jang et al., 2011; Kwon et al., 2011; Pan et al., 2012; Conti et al., 2014). However, comparative data concerning the feasibility and accuracy of fibre tracts assigned to different body parts are scarce: Hong et al. report similar FA values for hand and leg, using manually defined cortical ROIs without functional localizers (Hong et al., 2010b). To date, no data for nTMS-based CST fibre tracking have been published that compare distinct parameters of the different body-part-associated tracts. In this study, most plausible results were achieved for the hand fibre tracts on the unaffected hemisphere (CoHS–aiP algorithm: 100 %), followed by the CS fibre tracts originating from the CoHS of the hand (94%), the foot (81%) and at least the tongue (79%) on the side of the tumour. This finding may be a result of the higher retest-reliability and accuracy of hand motor mapping by nTMS as compared to the foot and the tongue representation (Forster et al., 2012; Weiss et al., 2013) which corresponds to a more exact cortical ROI delineation.

4.5. Analysis of influence factors on fibre course plausibility

4.5.1. Clinical and structural cofactors

For most clinical and radiological factors including tumour histology we could not detect significant correlations with fibre course plausibility. However, the presence of oedema within the PLIC had significant deleterious effects on the reconstruction of the CST, most evident for the CST fibres originating from the hand and the foot CoHS. Various papers have addressed the impact of tumours on DTI tracking (Lu et al., 2003; Min et al., 2013; Hoefnagels et al., 2014; Jones et al., 2014). Recently, Jones and colleagues have shown tumour-type-dependent diffusion characteristics with strongly reduced anisotropy in high-grade tumours and oedema (Jones et al., 2014). Interestingly, FA was shown to be significantly lower in tumour oedema as compared to a pure vasogenic oedema (Min et al., 2013). Low anisotropy values in an area representing a core zone of the CST such as the PLIC may explain the difficulties to achieve a valid tractography result in these cases.

4.5.2. FAT and MFL

The FA is a useful indicator for the validity of reconstructed fibre tracts since it describes the degree of directionality of the diffusion process and, hence, is widely accepted as a measure for structural white matter integrity (Basser and Pierpaoli, 1996, 2011; Chiang et al., 2014; Dacosta-Aguayo et al., 2014; Holtrop et al., 2014; Van der Werff et al., 2014). Not surprisingly, in this study, high FAT values showed a strong correlation with the plausibility of the tractography results. Moreover, a negative correlation of the FAT with the MFL was shown. Corrected for the influence of the MFL on the fibre course plausibility, the significant correlation of the FAT with the fibre course plausibility survived partial correlation analysis whereas the correlation 'MFL ~ plausibility' did not. Hence, FA seems to represent one of the strongest predictors for fibre course plausibility which was also confirmed by linear discriminant analysis (Coefficients of linear discriminants [cld]: cld[FAT] = 8.95, cld[MFL] = −.024). The less direct course of the reconstructed CST in cases of low FA may explain the prolonged MFL correlating with low FAT values. Hence, the correlation between MFL and fibre course plausibility may be interpreted as an epiphenomenon of its correlation with the respective FAT.

In order to provide a simple tool for clinical plausibility estimation based on the FAT (and MFL) of the respective tractography result, cut off even points were calculated (ROC analysis: FAT-plausibility: 0.105; MFL-plausibility: 121.5 mm) and illustrated by histograms and Kernel's density curves (Fig. 4). Hence, in case of FAT values lower or equal 0.10, it seems mandatory to interpret the tractography results with particular caution. MFL values exceeding 121.5 mm (field-of-view delineated by pontomedullary groove) may also be a negative predictor for plausible CST tractography, however, less powerful compared to the FAT value.

4.6. Intraoperative validation

4.6.1. Subcortical stimulation

As pointed out before, DTI-based tractography is a powerful technique which can facilitate function-preserving resection of rolandic brain tumours. However, the tracking algorithms are prone to artefacts, especially in areas with an unfavourable signal-to-noise ratio such as the surrounding of brain tumours. The tractography results should, therefore, always be interpreted with caution and, whenever possible, be confirmed intraoperatively. Subcortical monopolar stimulation provides an excellent tool to check the anatomical location of the respective fibre tracts (Duffau, 2007; Bello et al., 2008; Kombos et al., 2009; Sanai and Berger, 2010; Szelényi et al., 2011). One limitation of the present study is the lack of intraoperative stimulation data in order to validate the findings. A number of studies have already demonstrated that subcortical monopolar stimulation provides an excellent tool to check the anatomical location of the respective fibre tracts (Duffau, 2007; Bello et al., 2008; Kombos et al., 2009; Sanai and Berger, 2010; Szelényi et al., 2011). However, a major challenge of this technique is the non-linear brain shift after opening the skull which makes it impossible to use pre-operative MRIs as anatomical reference with sufficient spatial precision. This issue could, however, be clarified in the future by stereotactic approaches (Forster, 2015) or when using intraoperative MRI (Ostrý et al., 2013; Nimsky et al., 2005a, 2005b, 2006 and 2011; Shahar, 2014).

4.6.2. Awake surgery

Despite the advances of pre- and intraoperative imaging that have been made over the last decades, awake craniotomy should still be considered as a well tolerable (Beez et al., 2013) and the most robust functional monitoring approach for surgery of eloquently located brain tumours (Duffau et al., 2003; Pereira et al., 2009; De Benedictis et al., 2010; De Witt Hamer et al., 2012; Shinoura et al., 2013; Surbeck et al., 2015). Currently, the combination of pre- and intraoperative cortical and subcortical mapping techniques with awake surgery is largely considered ideal in order to optimize the extent of resection whilst preserving important brain function such as motor control (Duffau et al., 2003; Freyschlag and Duffau, 2014).

5. Conclusions

nTMS-based deterministic CST tractography is a feasible approach for presurgical delineation of the pyramidal tract in brain tumour patients. Due to its intuitive and relatively fast applicability, it can be well integrated into clinical routine. The results demonstrate clearly that anatomical seeding — in addition to the nTMS-derived cortical M1 ROI — at the anterior pontine level (aiP) leads to reliably more plausible tractography results compared to the use of a subcortical ROI defined by the posterior limb of the internal capsule (PLIC). Combining the ROIs (aiP, PLIC) did not lead to a significant benefit regarding plausibility but can, however, be helpful in particular cases.

In cases with FAT values lower than 0.10 and/or the presence of oedema within the PLIC, tractography results should be interpreted with particular caution. Moreover, long minimal fibre lengths (cut-off value: 121.5 mm) should be regarded a negative indicator regarding fibre course plausibility.

In this study, calculation of the somatotopic corticospinal fibre tracts originating from the hand M1 area showed most plausible results (tumour hemisphere: 94%; non-affected hemisphere 100%), followed by the foot (81%) and tongue-associated CST (75%). These findings may be explained by the more accurate and reliable detectability of the hand M1 representation by nTMS, as compared to the foot and the tongue and thus by supposedly more exact cortical seeding.

However, anatomically based plausibility analysis can only represent an estimative approach. Exact validation of the DTI-based CST tractography results is mandatory, e.g. by electrophysiological recordings during stereotactic procedures in functional neurosurgery.

Source of funding

We thank the German Research Foundation (DFG) for funding of the nTMS machine (Nexstim eXimia 4.2; grant nr. INST 1856/50-1).

Christian Grefkes is supported by the German Research Foundation (DFG GR 3285/2-1; GR 3285/4-1), and by the University of Cologne Emerging Groups Initiative (CONNECT group, implemented into the Institutional Strategy of the University of Cologne and the German Excellence Initiative).

Appendix A. Supplementary data

Supplementary data to this article can be found online at http://dx.doi.org/10.1016/j.nicl.2015.01.006.

References

Anand, S., Hotson, J., 2002. Transcranial magnetic stimulation: neurophysiological applications and safety. Brain Cogn. 50 (3), 366–386. http://dx.doi.org/10.1016/S0278-2626(02)00512-212480484.

Barbas, H., Pandya, D.N., 1987. Architecture and frontal cortical connections of the premotor cortex (area 6) in the rhesus monkey. J. Comp. Neurol. 256 (2), 211–228. http://dx.doi.org/10.1002/cne.9025602033558879.

Barone, D.G., Lawrie, T.A., Hart, M.G., 2014. Image guided surgery for the resection of brain tumours. Cochrane Database Syst. Rev. 1, CD009685. http://dx.doi.org/10.1002/14651858.CD009685.pub224474579.

Bashir, S., Perez, J.M., Horvath, J.C., Pascual-Leone, A., 2013. Differentiation of motor cortical representation of hand muscles by navigated mapping of optimal TMS current directions in healthy subjects. J. Clin. Neurophysiol. 30 (4), 390–395. http://dx.doi.org/10.1097/WNP.0b013e31829dda6b23912579.

Basser, P., Pierpaoli, C., 2011. Recollections about our 1996 JMR paper on diffusion anisotropy. J. Magn. Reson. 213 (2), 571–572. http://dx.doi.org/10.1016/j.jmr.2011.08.02322152372.

Basser, P.J., 1994. Focal magnetic stimulation of an axon. IEEE Trans. Biomed. Eng. 41 (6), 601–606. http://dx.doi.org/10.1109/10.2932487927380.

Basser, P.J., Pierpaoli, C., 1996. Microstructural and physiological features of tissues elucidated by quantitative-diffusion-tensor MRI. J. Magn. Reson. B 111 (3), 209–2198661285.

Basser, P.J., Pierpaoli, C., 1998. A simplified method to measure the diffusion tensor from seven MR images. Magn. Reson. Med. 39 (6), 928–934. http://dx.doi.org/10.1002/mrm.19103906109621916.

Basser, P.J., Roth, B.J., 2000. New currents in electrical stimulation of excitable tissues. Annu. Rev. Biomed. Eng. 2, 377–397. http://dx.doi.org/10.1146/annurev.bioeng.2.1.37711701517.

Beez, T., Boge, K., Wager, M., et al., 2013. Tolerance of awake surgery for glioma: a prospective European Low Grade Glioma Network multicenter study. Acta Neurochir. 155 (7), 1301–1308. http://dx.doi.org/10.1007/s00701-013-1759-023689968.

Bello, L., Gambini, A., Castellano, A., et al., 2008. Motor and language DTI fiber tracking combined with intraoperative subcortical mapping for surgical removal of gliomas. Neuroimage 39 (1), 369–382. http://dx.doi.org/10.1016/j.neuroimage.2007.08.03117911032.

Bucci, M., Mandelli, M.L., Berman, J.I., et al., 2013. Quantifying diffusion MRI tractography of the corticospinal tract in brain tumors with deterministic and probabilistic methods. Neuroimage Clin. 3, 361–368. http://dx.doi.org/10.1016/j.nicl.2013.08.00824273719.

Chiang, C.W., Wang, Y., Sun, P., et al., 2014. Quantifying white matter tract diffusion parameters in the presence of increased extra-fiber cellularity and vasogenic edema. Neuroimage 101, 310–319. http://dx.doi.org/10.1016/j.neuroimage.2014.06.06425017446.

Conti, A., Raffa, G., Granata, F., et al., 2014. Navigated transcranial magnetic stimulation for "somatotopic" tractography of the corticospinal tract. Neurosurgery 10 (Suppl 4), 542–554. http://dx.doi.org/10.1227/NEU.0000000000000050225072115.

Cowan, F.M., de Vries, L.S., 2005. The internal capsule in neonatal imaging. Semin. Fetal Neonatal. Med. 10 (5), 461–474. http://dx.doi.org/10.1016/j.siny.2005.05.007.

D'Andrea, G., Angelini, A., Romano, A., et al., 2012. Intraoperative DTI and brain mapping for surgery of neoplasm of the motor cortex and the corticospinal tract: our protocol and series in BrainSUITE. Neurosurg. Rev. 35 (3), 401–412. http://dx.doi.org/10.1007/s10143-012-0373-622370809.

Dacosta-Aguayo, R., Graña, M., Fernández-Andújar, M., et al., 2014. Structural integrity of the contralesional hemisphere predicts cognitive impairment in ischemic stroke at three months. PLOS One 9 (1), e86119. http://dx.doi.org/10.1371/journal.pone.008611924475078.

De Benedictis, A., Moritz-Gasser, S., Duffau, H., 2010. Awake mapping optimizes the extent of resection for low-grade gliomas in eloquent areas. Neurosurgery 66 (6), 1074–1084. http://dx.doi.org/10.1227/01.NEU.0000369514.74284.7820386138.

De Witt Hamer, P.C., Robles, S.G., Zwinderman, A.H., Duffau, H., Berger, M.S., 2012. Impact of intraoperative stimulation brain mapping on glioma surgery outcome: a meta-analysis. J. Clin. Oncol. 30 (20), 2559–2565. http://dx.doi.org/10.1200/JCO.2011.38.481822529254.

Duffau, H., 2007. Contribution of cortical and subcortical electrostimulation in brain glioma surgery: methodological and functional considerations. Neurophysiol Clin 37 (6), 373–382. http://dx.doi.org/10.1016/j.neucli.2007.09.00318083492.

Duffau, H., Capelle, L., Denvil, D., et al., 2003. Usefulness of intraoperative electrical subcortical mapping during surgery for low-grade gliomas located within eloquent brain regions: functional results in a consecutive series of 103 patients. J. Neurosurg. 98 (4), 764–778. http://dx.doi.org/10.3171/jns.2003.98.4.076412691401.

Forster, M.T., Hoecker, A.C., Kang, J.S., Quick, J., Seifert, V., Hattingen, E., Hilker, R., Weise, L.M., 2015. Does nTMS increase the accuracy of tractography? - A prospective clinical trial based on intraoperative MEP monitoring during DBS. Neurosurgery.

Forster, M.T., Senft, C., Hattingen, E., et al., 2012. Motor cortex evaluation by nTMS after surgery of central region tumors: a feasibility study. Acta Neurochir. 154 (8), 1351–1359. http://dx.doi.org/10.1007/s00701-012-1403-422669201.

Frey, D., Strack, V., Wiener, E., et al., 2012. A new approach for corticospinal tract reconstruction based on navigated transcranial stimulation and standardized fractional anisotropy values. Neuroimage 62 (3), 1600–1609. http://dx.doi.org/10.1016/j.neuroimage.2012.05.05922659445.

Freyschlag, C.F., Duffau, H., 2014. Awake brain mapping of cortex and subcortical pathways in brain tumor surgery. J. Neurosurg. Sci. 58 (4), 199–21325418274.

Gerardin, E., Lehéricy, S., Pochon, J.B., et al., 2003. Foot, hand, face and eye representation in the human striatum. Cereb. Cortex 13 (2), 162–169. http://dx.doi.org/10.1093/cercor/13.2.16212507947.

Greiner, M., Pfeiffer, D., Smith, R.D., 2000. Principles and practical application of the receiver—operating characteristic analysis for diagnostic tests. Prev. Vet. Med. 45 (1–2), 23–41. http://dx.doi.org/10.1016/S0167-5877(00)00115-X10802332.

Guye, M., Parker, G.J., Symms, M., et al., 2003. Combined functional MRI and tractography to demonstrate the connectivity of the human primary motor cortex in vivo. Neuroimage 19 (4), 1349–1360. http://dx.doi.org/10.1016/S1053-8119(03)00165-412948693.

Hajian-Tilaki, K., 2013. Receiver operating characteristic (ROC) curve analysis for medical diagnostic test evaluation. Caspian J Intern Med 4 (2), 627–63524009950.

Han, B.S., Hong, J.H., Hong, C., et al., 2010. Location of the corticospinal tract at the corona radiata in human brain. Brain Res. 1326, 75–80. http://dx.doi.org/10.1016/j.brainres.2010.02.05020219443.

Hendler, T., Pianka, P., Sigal, M., et al., 2003. Delineating gray and white matter involvement in brain lesions: three-dimensional alignment of functional magnetic resonance and diffusion-tensor imaging. J. Neurosurg. 99 (6), 1018–1027. http://dx.doi.org/10.3171/jns.2003.99.6.101814705730.

Herbsman, T., Forster, L., Molnar, C., et al., 2009. Motor threshold in transcranial magnetic stimulation: the impact of white matter fiber orientation and skull-to-cortex distance. Hum. Brain Mapp. 30 (7), 2044–2055. http://dx.doi.org/10.1002/hbm.2064918973261.

Hoefnagels, F.W., De Witt Hamer, P., Sanz-Arigita, E., et al., 2014. Differentiation of edema and glioma infiltration: proposal of a DTI-based probability map. J. Neurooncol. 120 (1), 187–198. http://dx.doi.org/10.1007/s11060-014-1544-925079117.

Holodny, A.I., Gor, D.M., Watts, R., et al., 2005b. Diffusion-tensor MR tractography of somatotopic organization of corticospinal tracts in the internal capsule: initial anatomic results in contradistinction to Prior reports. Radiology 234 (3), 649–653. http://dx.doi.org/10.1148/radiol.234303208715665224.

Holodny, A.I., Watts, R., Korneinko, V.N., et al., 2005a. Diffusion tensor tractography of the motor white matter tracts in man: current controversies and future directions. Ann. N. Y. Acad. Sci. 1064, 88–97. http://dx.doi.org/10.1196/annals.1340.01616394150.
Holtrop, J.L., Loucks, T.M., Sosnoff, J.J., Sutton, B.P., 2014. Investigating age-related changes in fine motor control across different effectors and the impact of white matter integrity. Neuroimage 96, 81–87. http://dx.doi.org/10.1016/j.neuroimage.2014.03.04524657352.
Hong, J.H., Son, S.M., Jang, S.H., 2010a. Identification of spinothalamic tract and its related thalamocortical fibers in human brain. Neurosci. Lett. 468 (2), 102–105. http://dx.doi.org/10.1016/j.neulet.2009.10.07519879333.
Hong, J.H., Son, S.M., Jang, S.H., 2010b. Somatotopic location of corticospinal tract at pons in human brain: a diffusion tensor tractography study. Neuroimage 51 (3), 952–955. http://dx.doi.org/10.1016/j.neuroimage.2010.02.06320206703.
Ilmoniemi, R.J., Ruohonen, J., Karhu, J., 1999. Transcranial magnetic stimulation — a new tool for functional imaging of the brain. Crit. Rev. Biomed. Eng. 27 (3–5), 241–28410864281.
Jang, S.H., 2011. Somatotopic arrangement and location of the corticospinal tract in the brainstem of the human brain. Yonsei Med. J. 52 (4), 553–557. http://dx.doi.org/10.3349/ymj.2011.52.4.55321623594.
Jones, T.L., Byrnes, T.J., Yang, G., et al., 2014. Brain tumor classification using the diffusion tensor image segmentation (D-SEG) technique. Neuro-Oncology http://dx.doi.org/10.1093/neuonc/nou15925121771.
Julkunen, P., Säisänen, L., Danner, N., et al., 2009. Comparison of navigated and non-navigated transcranial magnetic stimulation for motor cortex mapping, motor threshold and motor evoked potentials. Neuroimage 44 (3), 790–795. http://dx.doi.org/10.1016/j.neuroimage.2008.09.04018976714.
Karnofsky, D.A., Burchenal, J.H., 1994. The clinical evaluation of chemotherapeutic agents in cancer. In: MacLeod, C.M. (Ed.), Evaluation of Chemotherapeutic Agents. Columbia University Press, New York, p. 196.
Kombos, T., Süss, O., Vajkoczy, P., 2009. Subcortical mapping and monitoring during insular tumor surgery. Neurosurg. Focus 27 (4), E5. http://dx.doi.org/10.3171/2009.8.FOCUS0914019795954.
Koyama, T., Marumoto, K., Domen, K., et al., 2013. White matter characteristics of idiopathic normal pressure hydrocephalus: a diffusion tensor tract-based spatial statistic study. Neurol. Med. Chir. (Tokyo) 53, 601–60824067771.
Krieg, S.M., Buchmann, N.H., Gempt, J., et al., 2012. Diffusion tensor imaging fiber tracking using navigated brain stimulation—a feasibility study. Acta Neurochir. 154 (3), 555–563. http://dx.doi.org/10.1007/s00701-011-1255-322270529.
Kwon, H.G., Hong, J.H., Jang, S.H., 2011. Anatomic location and somatotopic arrangement of the corticospinal tract at the cerebral peduncle in the human brain. AJNR Am. J. Neuroradiol. 32 (11), 2116–2119. http://dx.doi.org/10.3174/ajnr.A266021903908.
Lazar, M., Weinstein, D.M., Tsuruda, J.S., et al., 2003. White matter tractography using diffusion tensor deflection. Hum Brain Mapp 18 (4), 306–321. http://dx.doi.org/10.1002/hbm.1010212632468.
Le Bihan, D., Mangin, J.F., Poupon, C., et al., 2001. Diffusion tensor imaging: concepts and applications. J. Magn. Reson. Imaging 13 (4), 534–546. http://dx.doi.org/10.1002/jmri.107611276097.
Lehéricy, S., Duffau, H., Cornu, P., et al., 2000. Correspondence between functional magnetic resonance imaging somatotopy and individual brain anatomy of the central region: comparison with intraoperative stimulation in patients with brain tumors. J. Neurosurg. 92 (4), 589–598. http://dx.doi.org/10.3171/jns.2000.92.4.058910761647.
List, J., Kübke, J.C., Lindenberg, R., et al., 2013. Relationship between excitability, plasticity and thickness of the motor cortex in older adults. Neuroimage 83, 809–816. http://dx.doi.org/10.1016/j.neuroimage.2013.07.03323876242.
Lu, S., Ahn, D., Johnson, G., Cha, S., 2003. Peritumoral diffusion tensor imaging of high-grade gliomas and metastatic brain tumors. AJNR Am. J. Neuroradiol. 24 (5), 937–94112748097.
Machii, K., Cohen, D., Ramos-Estebanez, C., Pascual-Leone, A., 2006. Safety of rTMS to non-motor cortical areas in healthy participants and patients. Clin. Neurophysiol. 117 (2), 455–471. http://dx.doi.org/10.1016/j.clinph.2005.10.01416387549.
Mandelli, M.L., Berger, M.S., Bucci, M., et al., 2014. Quantifying accuracy and precision of diffusion MR tractography of the corticospinal tract in brain tumors. J. Neurosurg. 121 (2), 349–358. http://dx.doi.org/10.3171/2014.4.JNS13116024905560.
Matelli, M., Luppino, G., Fogassi, L., Rizzolatti, G., 1989. Thalamic input to inferior area 6 and area 4 in the macaque monkey. J. Comp. Neurol. 280 (3), 468–488. http://dx.doi.org/10.1002/cne.9028003112537345.
McNemar, Q., 1947. Note on the sampling error of the difference between correlated proportions or percentages. Psychometrika 12 (2), 153–157. http://dx.doi.org/10.1007/BF02295996202254758.
Min, Z.G., Niu, C., Rana, N., et al., 2013. Differentiation of pure vasogenic edema and tumor-infiltrated edema in patients with peritumoral edema by analyzing the relationship of axial and radial diffusivities on 3.0T MRI. Clin. Neurol. Neurosurg. 115 (8), 1366–1370. http://dx.doi.org/10.1016/j.clineuro.2012.12.03123351840.
Mori, S., Crain, B.J., Chacko, V.P., van Zijl, P.C., 1999. Three-dimensional tracking of axonal projections in the brain by magnetic resonance imaging. Ann. Neurol. 45 (2), 265–269. http://dx.doi.org/10.1002/1531-8249(199902)45:2<265::AID-ANA21>3.0.CO;2-39989633.
Mori, S., Kaufmann, W.E., Davatzikos, C., et al., 2002. Imaging cortical association tracts in the human brain using diffusion-tenser-based axonal tracking. Magn. Reson. Med. 47 (2), 215–223. http://dx.doi.org/10.1002/mrm.1007411810663.
Mori, S., van Zijl, P.C., 2002. Fiber tracking: principles and strategies — a technical review. NMR Biomed. 15 (7–8), 468–480. http://dx.doi.org/10.1002/nbm.78112489096.
Muellbacher, W., Boroojerdi, B., Ziemann, U., Hallett, M., 2001. Analogous corticocortical inhibition and facilitation in ipsilateral and contralateral human motor cortex representations of the tongue. J. Clin. Neurophysiol. 18 (6), 550–558. http://dx.doi.org/10.1097/00004691-200111000-0000511779968.
Nagae-Poetscher, L.M., Jiang, H., Wakana, S., et al., 2004. High-resolution diffusion tensor imaging of the brain stem at 3 T. AJNR Am. J. Neuroradiol. 25 (8), 1325–133015466326.
Nimsky, C., 2011. Intraoperative acquisition of fMRI and DTI. Neurosurg. Clin. N. Am. 22 (2), 269–277. http://dx.doi.org/10.1016/j.nec.2010.11.00521435576.
Nimsky, C., Ganslandt, O., Hastreiter, P., et al., 2005a. Intraoperative diffusion-tensor MR imaging: shifting of white matter tracts during neurosurgical procedures – initial experience. Radiology 234 (1), 218–225. http://dx.doi.org/10.1148/radiol.234103198415564394.
Nimsky, C., Ganslandt, O., Hastreiter, P., et al., 2005b. Preoperative and intraoperative diffusion tensor imaging-based fiber tracking in glioma surgery. Neurosurgery 56 (1), 130–137. http://dx.doi.org/10.1227/01.neu.0000279214.00139.3b15617595.
Nimsky, C., Ganslandt, O., Merhof, D., et al., 2006. Intraoperative visualization of the pyramidal tract by diffusion-tensor-imaging-based fiber tracking. Neuroimage 30 (4), 1219–1229. http://dx.doi.org/10.1016/j.neuroimage.2005.11.00116364659.
Ohue, S., Kohno, S., Inoue, A., et al., 2012. Accuracy of diffusion tensor magnetic resonance imaging-based tractography for surgery of gliomas near the pyramidal tract: a significant correlation between subcortical electrical stimulation and postoperative tractography. Neurosurgery 70 (2), 283–294. http://dx.doi.org/10.1227/NEU.0b013e31823020e621811189.
Orioli, P.J., Strick, P.L., 1989. Cerebellar connections with the motor cortex and the arcuate premotor area: an analysis employing retrograde transneuronal transport of WGA-HRP. J. Comp. Neurol. 288 (4), 612–626. http://dx.doi.org/10.1002/cne.9028804082478593.
Ostrý, S., Belšan, T., Otáhal, J., et al., 2013. Is intraoperative diffusion tensor imaging at 3.0T comparable to subcortical corticospinal tract mapping? Neurosurgery 73 (5), 797–807. http://dx.doi.org/10.1227/NEU.0000000000000008723863765.
Pajevic, S., Pierpaoli, C., 1999. Color schemes to represent the orientation of anisotropic tissues from diffusion tensor data: application to white matter fiber tract mapping in the human brain. Magn. Reson. Med. 42 (3), 526–54010467297.
Pan, C., Peck, K.K., Young, R.J., Holodny, A.I., 2012. Somatotopic organization of motor pathways in the internal capsule: a probabilistic diffusion tractography study. AJNR Am. J. Neuroradiol. 33 (7), 1274–1280. http://dx.doi.org/10.3174/ajnr.A295222460344.
Park, C.H., Kou, N., Boudrias, M.H., et al., 2013. Assessing a standardised approach to measuring corticospinal integrity after stroke with DTI. Neuroimage Clin. 2, 521–533. http://dx.doi.org/10.1016/j.nicl.2013.04.00224179804.
Park, J.K., Kim, B.S., Choi, G., et al., 2008. Evaluation of the somatotopic organization of corticospinal tracts in the internal capsule and cerebral peduncle: results of diffusion-tensor MR tractography. Korean J. Radiol. 9 (3), 191–195. http://dx.doi.org/10.3348/kjr.2008.9.3.19118525220.
Parmar, H., Sitoh, Y.Y., Yeo, T.T., 2004. Combined magnetic resonance tractography and functional magnetic resonance imaging in evaluation of brain tumors involving the motor system. J. Comput. Assist. Tomogr. 28 (4), 551–556. http://dx.doi.org/10.1097/00004728-200407000-0001915232390.
Penfield, W., Rasmussen, T., 1950. The Cerebral Cortex of Man: A Clinical Study of Localization of Function. Macmillan, New York.
Pereira, L.C., Oliveira, K.M., L'Abbate, G.L., et al., 2009. Outcome of fully awake craniotomy for lesions near the eloquent cortex: analysis of a prospective surgical series of 79 supratentorial primary brain tumors with long follow-up. Acta Neurochir. (Wien) 151 (10), 1215–1230. http://dx.doi.org/10.1007/s00701-009-0363-919730779.
Petrides, M., Pandya, D.N., 1984. Projections to the frontal cortex from the posterior parietal region in the rhesus monkey. J. Comp. Neurol. 228 (1), 105–116. http://dx.doi.org/10.1002/cne.9022801106480903.
Picht, T., Mularski, S., Kuehn, B., et al., 2009. Navigated transcranial magnetic stimulation for preoperative functional diagnostics in brain tumor surgery. Neurosurgery 65 (6 Suppl), 93–99. http://dx.doi.org/10.1227/01.NEU.0000348009.22750.5919935007.
Picht, T., Schmidt, S., Brandt, S., et al., 2011. Preoperative functional mapping for rolandic brain tumor surgery: comparison of navigated transcranial magnetic stimulation to direct cortical stimulation. Neurosurgery 69 (3), 581–588. http://dx.doi.org/10.1227/NEU.0b013e3182181b8921430587.
Picht, T., Schulz, J., Hanna, M., et al., 2012. Assessment of the influence of navigated transcranial magnetic stimulation on surgical planning for tumors in or near the motor cortex. Neurosurgery 70 (5), 1248–1256. http://dx.doi.org/10.1227/NEU.0b013e318243881e22127045.
Prabhu, S.S., Gasco, J., Tummala, S., et al., 2011. Intraoperative magnetic resonance imaging-guided tractography with integrated monopolar subcortical functional mapping for resection of brain tumors. Clinical article. J. Neurosurg. 114 (3), 719–726. http://dx.doi.org/10.3171/2010.9.JNS1048120964594.
Rödel, R., Laskawi, R., Markus, H., Neupert, P., 1999. [Possible one-dimensional determination of cortical representative fields of mimetic lower lip muscles by transcranial magnetic stimulation]. Laryngorhinootologie 78 (10), 552–556. http://dx.doi.org/10.1055/s-1999-875610595339.
Rödel, R.M., Laskawi, R., Markus, H., 2003. Tongue representation in the lateral cortical motor region of the human brain as assessed by transcranial magnetic stimulation. Ann. Otol. Rhinol. Laryngol. 112 (1), 71–76. http://dx.doi.org/10.1177/000348940311200114125370 62.
Romano, A., D'Andrea, G., Calabria, L.F., et al., 2011. Pre- and intraoperative tractographic evaluation of corticospinal tract shift. Neurosurgery 69 (3), 696–705. http://dx.doi.org/10.1227/NEU.0b013e31821a855521471830.
Rossi, S., Hallett, M., Rossini, P.M., et al., 2009. Safety, ethical considerations, and application guidelines for the use of transcranial magnetic stimulation in clinical practice and research. Clin. Neurophysiol. 120 (12), 2008–2039. http://dx.doi.org/10.1016/j.clinph.2009.08.01619833552.

Rossini, P.M., Barker, A.T., Berardelli, A., et al., 1994. Non-invasive electrical and magnetic stimulation of the brain, spinal cord and roots: basic principles and procedures for routine clinical application. Report of an IFCN committee. Electroencephalogr. Clin. Neurophysiol. 91 (2), 79–92. http://dx.doi.org/10.1016/0013-4694(94)90029-97519144.

Roth, Y., Pell, G.S., Chistyakov, A.V., et al., 2014. Motor cortex activation by H-coil and figure-8 coil at different depths. Combined motor threshold and electric field distribution study. Clin. Neurophysiol. 125 (2), 336–343. http://dx.doi.org/10.1016/j.clinph.2013.07.01323994191.

Säisänen, L., Julkunen, P., Niskanen, E., et al., 2008. Motor potentials evoked by navigated transcranial magnetic stimulation in healthy subjects. J. Clin. Neurophysiol. 25 (6), 367–372. http://dx.doi.org/10.1097/WNP.0b013e31818e7944.

Sanai, N., Berger, M.S., 2010. Intraoperative stimulation techniques for functional pathway preservation and glioma resection. Neurosurg. Focus 28 (2), E1. http://dx.doi.org/10.3171/2009.12.FOCUS0926620121436.

Schonberg, T., Pianka, P., Hendler, T., et al., 2006. Characterization of displaced white matter by brain tumors using combined DTI and fMRI. Neuroimage 30 (4), 1100–1111. http://dx.doi.org/10.1016/j.neuroimage.2005.11.01516427322.

Seo, J.P., Jang, S.H., 2013. Characteristics of corticospinal tract area according to pontine Level. Yonsei Med. J. 54 (3), 785–787. http://dx.doi.org/10.3349/ymj.2013.54.3.78523549830.

Shahar, T., Rozovski, U., Marko, N.F., Tummala, S., Ziu, M., Weinberg, J.S., Rao, G., Kumar, V.A., Sawaya, R., Prabhu, S.S., 2014. Preoperative imaging to predict intraoperative changes in tumor-to-corticospinal tract distance: an analysis of 45 cases using high-field intraoperative magnetic resonance imaging. Neurosurgery 75 (1), 23–30. http://dx.doi.org/10.1227/NEU.0000000000000033824618800.

Shinoura, N., Midorikawa, A., Yamada, R., et al., 2013. Awake craniotomy for brain lesions within and near the primary motor area: a retrospective analysis of factors associated with worsened paresis in 102 consecutive patients. Surg. Neurol. Int. 4, 149. http://dx.doi.org/10.4103/2152-7806.12200324381792.

Staempfli, P., Reischauer, C., Jaermann, T., et al., 2008. Combining fMRI and DTI: a framework for exploring the limits of fMRI-guided DTI fiber tracking and for verifying DTI-based fiber tractography results. Neuroimage 39 (1), 119–126. http://dx.doi.org/10.1016/j.neuroimage.2007.08.02517931889.

Strick, P.L., Preston, J.B., 1983. Input–output organization of the primate motor cortex. Adv. Neurol. 39, 321–3276660099.

Surbeck, W., Hildebrandt, G., Duffau, H., 2015. The evolution of brain surgery on awake patients. Acta Neurochir. 157 (1), 77–84. http://dx.doi.org/10.1007/s00701-014-2249-825352088.

Szelényi, A., Senft, C., Jardan, M., et al., 2011. Intra-operative subcortical electrical stimulation: a comparison of two methods. Clin. Neurophysiol. 122 (7), 1470–1475. http://dx.doi.org/10.1016/j.clinph.2010.12.05521330203.

Tassinari, C.A., Cincotta, M., Zaccara, G., Michelucci, R., 2003. Transcranial magnetic stimulation and epilepsy. Clin. Neurophysiol. 114 (5), 777–798. http://dx.doi.org/10.1016/S1388-2457(03)00004-X12738425.

Roedel, R.M., Laskawi, R., Markus, H., 2001. Cortical representation of the orbicularis oculi muscle as assessed by transcranial magnetic stimulation (TMS). Laryngoscope 111 (11 1), 2005–2011. http://dx.doi.org/10.1097/00005537-200111000-0002611801987.

Van der Werff, S.J., Andela, C.D., Nienke Pannekoek, J., et al., 2014. Widespread reductions of white matter integrity in patients with long-term remission of Cushing's disease. Neuroimage Clin. 4, 659–667. http://dx.doi.org/10.1016/j.nicl.2014.01.01724936417.

Vassal, F., Schneider, F., Nuti, C., 2013. Intraoperative use of diffusion tensor imaging-based tractography for resection of gliomas located near the pyramidal tract: comparison with subcortical stimulation mapping and contribution to surgical outcomes. Br. J. Neurosurg. 27 (5), 668–675. http://dx.doi.org/10.3109/02688697.2013.77173023458557.

Watts, R., Liston, C., Niogi, S., Uluğ, A.M., 2003. Fiber tracking using magnetic resonance diffusion tensor imaging and its applications to human brain development. Ment. Retard. Dev. Disabil. Res. Rev. 9 (3), 168–177. http://dx.doi.org/10.1002/mrdd.1007712953296.

Wehner, T., 2013. The role of functional imaging in the tumor patient. Epilepsia 54 (Suppl. 9), 44–49. http://dx.doi.org/10.1111/epi.1244324328872.

Weiss, C., Nettekoven, C., Rehme, A.K., et al., 2013. Mapping the hand, foot and face representations in the primary motor cortex — retest reliability of neuronavigated TMS versus functional MRI. Neuroimage 66, 531–542. http://dx.doi.org/10.1016/j.neuroimage.2012.10.04623116812.

Wengenroth, M., Blatow, M., Guenther, J., et al., 2011. Diagnostic benefits of presurgical fMRI in patients with brain tumours in the primary sensorimotor cortex. Eur. Radiol. 21 (7), 1517–1525. http://dx.doi.org/10.1007/s00330-011-2067-921271252.

Wu, J.S., Zhou, L.F., Tang, W.J., et al., 2007. Clinical evaluation and follow-up outcome of diffusion tensor imaging-based functional neuronavigation: a prospective, controlled study in patients with gliomas involving pyramidal tracts. Neurosurgery 61 (5), 935–948. http://dx.doi.org/10.1227/01.neu.0000303189.80049.ab18091270.

Yoshiura, T., Kumazawa, S., Noguchi, T., et al., 2008. MR tractography based on directional diffusion function validation in somatotopic organization of the pyramidal tract. Acad. Radiol. 15 (2), 186–192. http://dx.doi.org/10.1016/j.acra.2007.09.00918206617.

Yousry, T.A., Schmid, U.D., Alkadhi, H., et al., 1997. Localization of the motor hand area to a knob on the precentral gyrus. A new landmark. Brain 120 (1), 141–157. http://dx.doi.org/10.1093/brain/120.1.1419055804.

Zhu, F.P., Wu, J.S., Song, Y.Y., et al., 2012. Clinical application of motor pathway mapping using diffusion tensor imaging tractography and intraoperative direct subcortical stimulation in cerebral glioma surgery: a prospective cohort study. Neurosurgery 71 (6), 1170–1184. http://dx.doi.org/10.1227/NEU.0b013e318271bc6122986591.

Zolal, A., Hejcl, A., Malucelli, A., et al., 2013. Distant white-matter diffusion changes caused by tumor growth. J. Neuroradiol. 40 (2), 71–80. http://dx.doi.org/10.1016/j.neurad.2012.05.00623433909.